A&A 436, 763–784 (2005)
DOI: 10.1051/0004-6361:20041815
© ESO 2005

Astronomy & Astrophysics

Resonant absorption troughs in the gamma-ray spectra of QSO⋆,⋆⋆,⋆⋆⋆

A. F. Iyudin[1], O. Reimer[2], V. Burwitz[1], J. Greiner[1], and A. Reimer[2]

[1] Max-Planck-Institut für extraterrestrische Physik, Postfach 1312, 85741 Garching, Germany
e-mail: [ani;burwitz;jcg]@mpe.mpg.de
[2] Institut für Theoretische Physik, Lehrstuhl IV: Weltraum- und Astrophysik, Ruhr-Universität Bochum, 44780 Bochum, Germany

Received 9 August 2004 / Accepted 11 February 2005

Abstract. We report the very first evidence of the possible detection of γ-ray resonant absorption along the line of sight towards γ-ray bright quasars (QSOs), like 3C 279, 3C 273, PKS 0528+0134, and BL Lacertae. These detections resulted from the analysis of COMPTEL and EGRET data that were collected either during monitoring campaigns of the Virgo and galactic anticenter regions by the Compton Gamma Ray Observatory (CGRO) or during ToO observations of QSOs flares.
We discuss three resonant absorption mechanisms that affect the γ-ray spectrum of point-like sources when crossing the surrounding warm and cold absorbers, as well as the potential of this γ-ray photon absorption method to constrain the abundance of the absorber. We detected two absorbers along the line of sight towards γ-ray bright QSOs, one at the QSO rest frame redshift and another at approximately zero redshift. We tentatively identify the latter with an absorber in the Galactic halo, while the former is undoubtedly caused by photon absorption in the host galaxy of the QSO.
We discuss the advantages and drawbacks of this method in studies of absorbers in different astrophysical environments and compare this new method to absorber studies at X-ray or other wavelengths. We applied this γ-ray absorption method to identify a few of the EGRET unidentified (EUID) sources as QSOs, and determine their redshifts.

Key words. galaxies: active – galaxies: quasars: absorption lines – gamma-rays: observations – ISM: general

1. Introduction

The detection of resonant absorption lines is the most frequently used tool today for studying the intervening matter at low and high redshifts. Recently, quite a number of absorption line detections were reported along the line of sight of 3C 273 in X-rays (Fang et al. 2003), as well as in the optical and ultraviolet (Savage et al. 2000; Tripp et al. 2000; Savage et al. 2003, and references therein). Other objects, like PKS 2155-304, have also been shown to have absorption lines from highly ionized O VII (and O VIII) (Nicastro et al. 2002; Fang et al. 2002). For instance, in the 900 ks long *Chandra* observation of the bright Seyfert galaxy NGC 3783, Kaspi et al. (2002) detected the O VII absorption line among many other lines of different ions of abundant elements C, N, O, Ne, Mg, Al, Si, S, and Fe. These detections of high-ionization species complement and expand upon previously discussed detections of galactic and intergalactic O VI on different lines of sight (Savage et al. 2000, 2003), as well as of C IV, Si IV, and N V (Savage et al. 2000; Tripp et al. 2000), e.g. absorption lines detected by the Far Ultraviolet Spectroscopic Explore (*FUSE*) and by the Hubble Space Telescope (*HST*).

Resonance line absorption troughs in UV and X-rays were used to detect and to contrast column densities of the outflowing matter in Seyferts (Arav et al. 1997; Arav et al. 2002; Arav et al. 2003). Because of the high penetrating power of X-rays, broad-band (0.1–10 keV) X-ray spectrometers are sensitive to column densities in the range 10^{19} to 5×10^{24} cm^{-2} (Nandra et al. 1997; George et al. 1998; Mushotzky 1997).

When studying absorption troughs of a given quasar (and ion) with either UV or X-ray observations, one finds that the optical depth derived from the UV line is always ~50 times smaller than the X-ray derived depth (Arav et al. 2002, 2003). This is a consequence of the wavelength difference between absorption lines in UV and X-rays for the same ion, which means that the X-ray troughs are sensitive to a much higher column density than those of the UV, and can be used to provide a saturation test for the UV troughs (Arav et al. 2003).

With the same line of arguments, γ-ray absorption is sensitive to even higher column densities, which thus can be used to test the saturation in the X-ray troughs. Additionally, the detection of γ-ray photon absorption in QSO environments may shed new light on the physics governing the QSO behaviour

⋆ *Present address*: Skobeltsyn Institute of Nuclear Physics, Moscow State University, Vorob'evy Gory, 119992 Moscow, Russia.

⋆⋆ The COMPTEL project was supported by the BMBF through DLR grant 50 QV 9096 8.

⋆⋆⋆ All appendices are only available in electronic form at http://www.edpsciences.org

Article published by EDP Sciences and available at http://www.edpsciences.org/aa or http://dx.doi.org/10.1051/0004-6361:20041815

during active periods (flares), and especially, on the QSO emission mechanism(s) at different energy regimes.

The only γ-ray absorption studies applied to QSOs or their surrounding medium have been performed at Very High-Energy γ-rays, i.e. at TeV energies, by the IR/O background radiation field (see Coppi & Aharonian 1999; Aharonian et al. 2001, and references therein). Also, only few theoretical investigations of the location of the GeV-source in QSOs have been undertaken, primarily to avoid absorption in the radiation field of the accretion disk (e.g. Dermer & Schlickeiser 1994).

We demonstrate below that a study of γ-ray absorption features in the spectra of bright QSOs (both time-averaged as well as flare only) is already feasible today with the available data of COMPTEL and EGRET, e.g. two γ-ray telescopes that have been flown onboard the Compton Gamma-Ray Observatory (CGRO). We verify the proposed gamma-ray absorption method using galactic sources that are bright in the MeV-GeV γ-ray energy range, like the Vela and Geminga pulsars.

The paper is organized as follows. In Sect. 2 we introduce major photoabsorption processes, while Sect. 3 presents instrument details and the basics of the spectral analysis. In Sect. 4 we present our results for γ-ray bright QSOs. Section 5 aims to demonstrate the capabilities of the photon absorption method when applied to the unidentified EGRET sources. We discuss our results in Sect. 6, and Sect. 7 gives a summary of this work. The Appendix provides the discussion of the relevant nuclear processes that lead to the resonant γ-ray absorption in general, including line-like absorption.

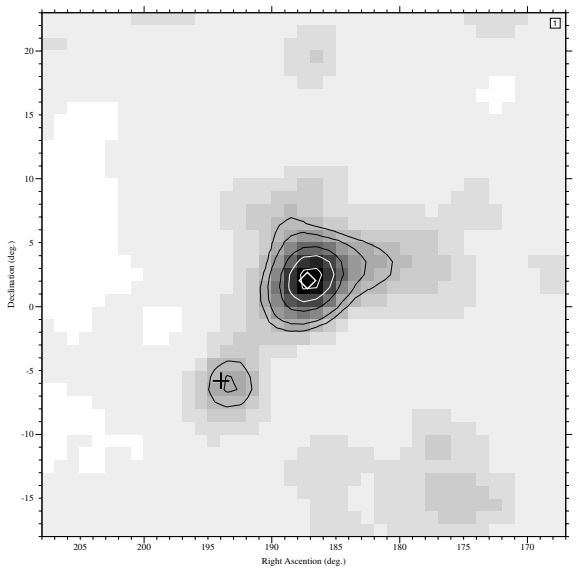

Fig. 1. COMPTEL image of the 3C 273 region in the energy range 4.3–10 MeV after the combination of all observations over the 9 yr CGRO mission lifetime. The position of 3C 273 is marked by a diamond, and the 3C 279 position is marked by a cross.

2. Cross section of γ-ray interaction with matter

In view of the potential importance of photon absorption troughs detected in the spectra of QSOs, we introduce the resonant photon absorption processes on nuclei here, and will discuss these processes in more detail in the Appendix.

It is well known that the most important processes for photon beam attenuation are the photo-effect for photon energies $\leq$100 keV in gaseous matter, followed by Compton scattering in the energy range of 100 keV $< E_\gamma <$ 10 MeV, and finally by e^+e^- pair production at higher energies (see, for example, Hubbell 1971; Hubbell et al. 1986).

At photon energies above $\approx$100 keV, both high-energy attenuation processes, Compton scattering and pair production, have a rather smooth functional dependence of the cross section on the photon energy (Hubbell 1971). These dependences are used in modern telescopes developed to study different astrophysical phenomena in the gamma rays (Chupp 1976; Fichtel & Trombka 1981).

At the same time in the nuclear physics community, it is well known that the total absorption cross section of photons by nuclei have three energy bands with resonant-like features in the cross section, namely at energies of ~7 MeV ("pygmy" dipole resonance (PDR) region), 20–30 MeV (giant dipole resonance (GDR) region), and ~325 MeV (Δ-resonance region) (Hayward 1977; Ahrens 1985). The two best studied of these three regions are the giant dipole resonance (GDR) region and the Δ-isobar region (Fig. 1 in Ahrens 1985). The total photon absorption cross section of nuclei has a nearly zero value at the energy slightly below the pion mass of ~140 MeV, and is rather small in the "shadow" region, i.e. at $E_\gamma \geq 2$ GeV. For the lightest nuclei after the Δ-resonance, one can see also a small bump related to the N^*-resonance production at $E_\gamma \sim 750$ MeV, which is most pronounced in the photon-hydrogen interactions (Fig. A.1). For heavier nuclei this resonance is smeared due to the "shadow" effect, i.e. nucleons are shadowing each other in the nuclei; and this interference leads to almost zero value of the N^*-resonance cross section of heavy nuclei (Ahrens 1985). For example, only a shoulder-like excess can be seen for N^*-resonance in the cross section of ^{4}He (Fig. A.2), while this shoulder completely disappears for ^{27}Al (Fig. A.3) and heavier nuclei.

Contribution of the resonant photo-absorption processes of nuclei relatively to the total photon attenuation varies from 2% to 9% for the GDR, depending on the nuclei mass number and nuclear structure (Hubbell 1971), and it is smaller for Δ-resonance absorption.

The third energy region with the resonant behaviour of the photon absorption cross section is located in the MeV region (around ~7 MeV) (Axel 1962; Hayward 1977; Bohr & Mottelson 1975; Suzuki et al. 1990; Van Isacker et al. 1992), i.e. below the threshold energies of the photoparticle production in reactions like (γ, n), (γ, p), and/or (γ, X).

3. Instruments and analysis technique

In the following we will discuss results acquired by two instruments on-board the Compton Gamma-Ray Observatory (CGRO), the COMPTEL and EGRET gamma-ray telescopes.

3.1. COMPTEL

COMPTEL aboard CGRO was the first generation γ-ray imaging telescope capable of performing an all-sky survey at MeV energies. COMPTEL operated in the 0.75–30.0 MeV energy range with a field of view of about 1 steradian, a source location accuracy of $\sim 1^\circ$ and an energy resolution of 5–10% *FWHM*. A detailed description of the instrument, its calibration, and COMPTEL data analysis in the 3-dimensional data space is given by Schönfelder et al. (1993).

The imaging data space of a Compton telescope is spanned by three coordinates, with two angles χ and ψ of the direction of the scattered γ-ray photon (the scatter direction) and the scatter angle ($\bar{\varphi}$) between the incoming and scattered photon. The scatter angle $\bar{\varphi}$ is calculated from measured energy losses in two detectors using the Compton-scatter formula, while angles χ and ψ are determined by the interaction locations of the γ-ray photon in the D1- and D2-detectors. The 3D data space binning is $1^\circ \times 1^\circ \times 2^\circ$ in χ, ψ, $\bar{\varphi}$. In COMPTEL imaging analyses, γ-ray albedo photons from the Earth's atmosphere are rejected by determining, for each event, the minimal angular distance, denoted by ζ, between its possible origins in the sky and the Earth horizon. The event selection set that was used in this paper differs in the minimum Earth-horizon event angle from the standard selection set (EHS178) used by the COMPTEL team. Our event criterion is more stringent, in the sense of more efficient, rejection of secondary γ-quanta coming from the Earth-horizon direction (see discussion on the selection set in Iyudin et al. 2004).

COMPTEL detected a variety of different types of objects, among them active galactic nuclei (AGN, like 3C 273 and 3C 279 shown in Fig. 1), pulsars, X-ray binaries, and supernova remnants (SNRs) (Schönfelder et al. 2000).

3.2. EGRET

EGRET was the high-energy gamma-ray telescope on-board CGRO. Descriptions of the instrument capabilities are given by Hughes et al. (1980), Kanbach et al. (1988), Nolan et al. (1992), and Thompson et al. (1993a). The telescope covers gamma-ray energies from about 20 MeV to above 20 GeV, with a broad maximum of the effective area of 1500 cm^2 in the range 500 MeV to 1 GeV. The sensitivity decreases with increasing off-axis angle approximately as a Gaussian with an HWHM of $\sim 20^\circ$. EGRET records γ-ray photons individually as electron-positron pair events, from which an arrival direction and the γ-photon energy are derived for each detected photon. The pair-production tracks obtained by the spark chamber allow for very good rejection of the instrument background. The results of pre-flight and in-flight calibrations are given by Thompson et al. (1993a) and Esposito et al. (1999).

3.3. Analysis of the COMPTEL data

For the present analysis, we have made use of a variant of the maximum-likelihood method (SRCFIX), as developed by van Dijk (1996). This is standard COMPTEL analysis software that has evolved from earlier work on the diffuse emission modeling in the COMPTEL data space. In this imaging program an internal background model is generated using a filtering technique for each observation, which takes into account the variation of the instrumental background with time. This technique is based on the fact that the (χ, ψ) structure of the data cube is well described to first order by the known geometry characteristics, with deviations largely independent of $\bar{\varphi}$ (Bloemen et al. 1994). Note that COMPTEL's instrumental background comprises ~98% of the total background in the 1–3 MeV energy interval, but it decreases significantly above an energy of ~4.3 MeV. An iterative approach (background modeling and sky-model fitting being performed simultaneously) was added to this method (Bloemen et al. 1999, 2000). In this latest approach all observations are again handled separately, in order to account for changes in the instrumental background during the mission.

In the following the display of the maximum-likelihood ratios over the field of view is referred to as the maximum-likelihood (ML) map. Such maps allow determination of the excess significance, flux, error region, etc. Figure 1 presents such a likelihood ratio contour map of the Virgo region in γ-rays of energy band 4.3–10.0 MeV, where two excesses are clearly detected, namely those of 3C 273 on the map center marked by a diamond and of 3C 279 to the south-east from 3C 273, marked by a cross.

This kind of map was used to produce spectral energy distributions (SEDs) of 3C 273 and 3C 279 (Collmar 2003) with standard COMPTEL energy bins (0.75–1.0 MeV, 1–3 MeV, 3–10 MeV, and 10–30 MeV) for the combination of all observations of 1991–1997 period of time. Because of the relative brightness of 3C 273 and 3C 279 we have also produced SEDs of these two QSOs with narrower energy bins (Fig. 2). By comparing the two sets of SEDs of 3C 273 and 3C 279, one can state that the narrow energy bin SEDs contain additional features at $E_\gamma \sim 7$ MeV, which are usually hidden in the SEDs based on the standard energy bins of COMPTEL, like those used in a paper summarizing the COMPTEL study of the 3C 273 region (Collmar 2003).

This absorption feature appears more significant with a confidence level of $\geq$0.99 for the case of 3C 273 ($z = 0.1584$, Strauss et al. 1992). But the spectrum of 3C 279 ($z = 0.536$) also shows some indication of an absorption feature at approximately the same energy. Since both features are at the same energy despite a factor 5 difference in redshift, they are probably produced by the PDR-like absorption on nuclei of a local absorber. Clearly, these results are worth following up with a higher energy instrument, like EGRET, and in a broader energy range that includes energies of other potential absorption features in the SED of a γ-bright QSO.

We conclude this subsection by saying that a more quantitative analysis of the feature detected by COMPTEL near the ~7 MeV (Fig. 2) has to await more detailed results of the ongoing studies of photon absorption on nuclei in this energy region (Hartmann et al. 2002), but the qualitative use of such a feature for the absorber redshift determination remains undoubtedly valid. Unfortunately, the number of objects having SEDs with absorption features in this energy range remains very small due

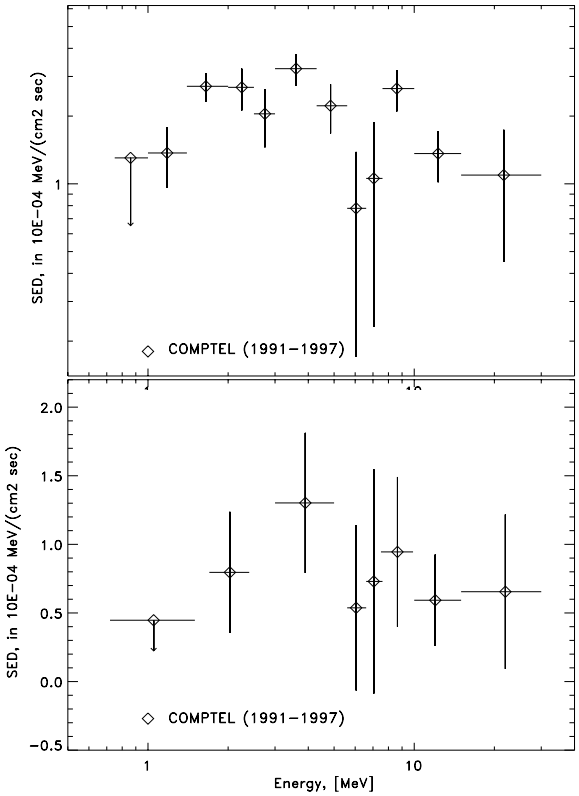

Fig. 2. 3C 273 (*top*) and 3C 279 (*bottom*) spectra derived by using the maximum-likelihood method for COMPTEL data covering observations of these two QSOs until March 1997. These spectra are generated with a smaller width of the energy bins as compared to the earlier standard analysis of the COMPTEL team. The error bars represent 1σ error.

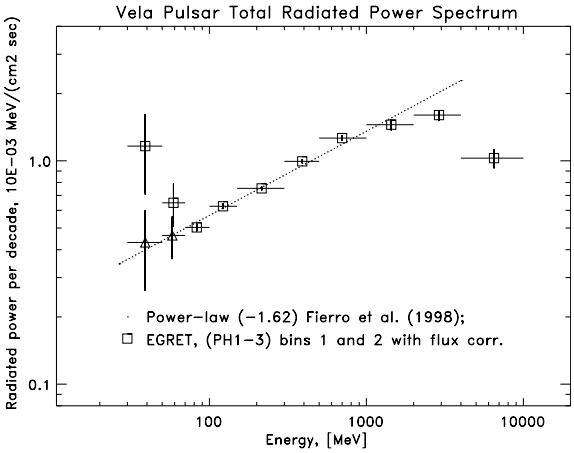

Fig. 3. Total Vela pulsar spectrum derived by using only the spatial analysis method for EGRET data, covering observations of Vela from 10 May 1991 till 4 October 1994, with usual selections (Fierro et al. 1998). The two lowest energy bins are shown with (boxes) and without flux correction factors (triangles).

to the low sensitivity of the gamma-ray telescopes used so far in this energy range.

3.4. Analysis of EGRET spectra

3.4.1. Standard procedure

The EGRET point source detection is based on the maximum likelihood analysis of the observed region (Mattox et al. 1996), under the assumption that the diffuse emission is a combination of an isotropic diffuse radiation plus a component produced by the cosmic-ray interactions in galactic atomic and molecular hydrogen gas (Bertsch et al. 1993; Hunter et al. 1997). The detection by EGRET is based on the point-source "test-statistic", which is defined as

$$T_{\rm s} \equiv -2\,(\ln L_0 - \ln L_1)\,. \qquad (1)$$

Here $T_{\rm s}$ is expected to be asymptotically distributed as χ^2_1 in the null hypothesis because of the one additional parameter of the alternative hypothesis. Because of the broad point spread function (PSF) of EGRET (5.85° at $E > 100$ MeV), the analysis is consistent with the χ^2_1 for cases with number (N) of detected photons from the point source with $N > 20$.

The ambiguity of the interpretation of an EGRET likelihood ratio test as a source detection or as an upper limit depends on the value of $T_{\rm s}^{1/2}$, as well as on the nature of the source. For the case of AGN usually a 4σ detection outside the galactic plane, and 5σ in the galactic plane suffices (Hartman et al. 1999). For the case with $T_{\rm s}^{1/2} < 1$ only an upper limit is provided, which is a 84% confidence flux upper limit in the spectral analysis (Mattox et al. 1996). Note, that in this study we generally use SEDs of AGN that were detected with rather high statistical significance (see Hartman et al. 1999).

In order to determine the γ-ray spectrum of the source of interest, the EGRET energy band of 30 MeV–10 GeV was divided into 10 bins. The number of source counts in each energy interval was determined by a maximum-likelihood analysis that includes a point source (QSO or other source), a model of the diffuse background, and the presence of the other known point source(s) in the field. The diffuse emission model of Hunter et al. (1997) is generally applied. Given the diffuse background model, the source strength was determined by simultaneously optimizing the likelihood probability function with normalization of the background model and the source strength(s) of other source(s) in the field, if present, as free parameters (Mattox et al. 1996).

3.4.2. Analysis of the EGRET spectra

Before proceeding with the analysis of EGRET QSO spectra, we need to recapitulate the flux calibration of the two lowest energy bins of EGRET, at 30–50 MeV and 50–70 MeV. Looking at the spectra of bright sources detected by EGRET, such as pulsars, the two lowest energy points in the spectra are often quite off the single power-law spectral fit. One can see this effect, for example, in papers by Thompson et al. (1997), Fierro et al. (1998), as well as in our Figs. 3–5. The two lowest energy bins in the EGRET spectra are subjected to a flux normalization using correction coefficients that were introduced by the EGRET Team as a consequence of discrepancies between the beam calibration and the actual flight performance of the instrument (Thompson et al. 1993b). This renormalization was based on a comparison of the early EGRET

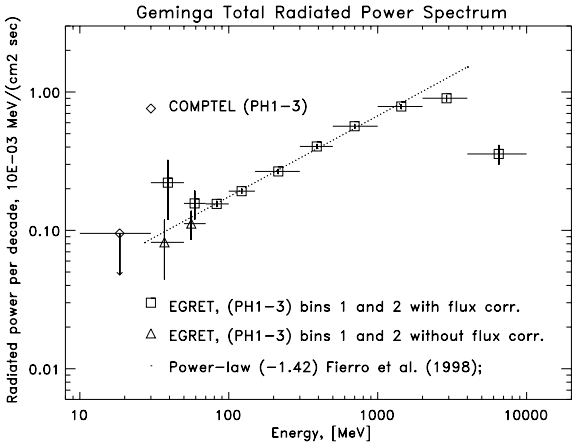

Fig. 4. Total Geminga spectrum derived by using spatial analysis method for EGRET data (Fierro et al. 1998) covering observations from 10 May 1991 until 4 October 1994. COMPTEL's upper limit for 10–30 MeV energy bin shown by the diamond is from paper by Kuiper et al. (1996).

spectrum of the Crab Nebula with the spectrum composed of the COMPTEL data and data of instruments flown before CGRO, like HEAO-3, HEAO-4, COS-B, MIFRASO, FIGARO, etc., see Strong et al. (1993), i.e., the spectrum that was believed to achieve a spectral match over the energies in question. Since these correction coefficients have no convincing physical explanation, we take the freedom to fit our model to two variants of the EGRET spectra: one with and another without these correction factors applied to the two lowest energy bins.

We selected two γ-ray bright, nearby pulsars, namely Vela (distance of ∼400 pc from the Sun; Cha & Sembach 2000; Pozzo et al. 2000) and Geminga (distance of ∼160 pc; Caraveo et al. 1996) to avoid effects that may be caused by the intervening galactic matter between the object and the observer. Indeed, we have found no hint of the absorption in the spectra of both pulsars at the energy of outmost interest of ∼325 MeV, e.g. at an energy of the Δ-resonance absorption (see Appendix).

We find that single power-law fits to the Vela and Geminga total emission spectra are significantly better representations under omission of the flux corrections coefficients in the two lowest energy points (Figs. 3 and 4). Our approach of not using these flux correction coefficients for EGRET is also supported by the available COMPTEL points in the Vela spectra of phases P1 and P2 (Fig. 5), or in the case of Geminga, by the total emission spectrum with the upper limit for the adjacent energy interval of 10–30 MeV provided by COMPTEL (Fig. 4). The improvement of the power-law fit of both pulsar's spectra is a decrease in the χ^2 value after omitting the low energy bin flux correction by 4.54, 4.27 and 1.7 for the Vela total emission, pulsed P1 and pulsed P2 spectra, respectively. The improvement to the fit for the Geminga spectrum can be characterized by $\Delta\chi^2 \sim 1.5$. All $\Delta\chi^2$ values are admittedly quite small, but consistently have the same sign.

Even for the more complicated spectral fit of the Crab Nebula, the fit is also better without the correction factors, but the fit is dependent on the SED model used (Atoyan & Aharonian 1996; de Jager et al. 1996; Kuiper et al. 2001).

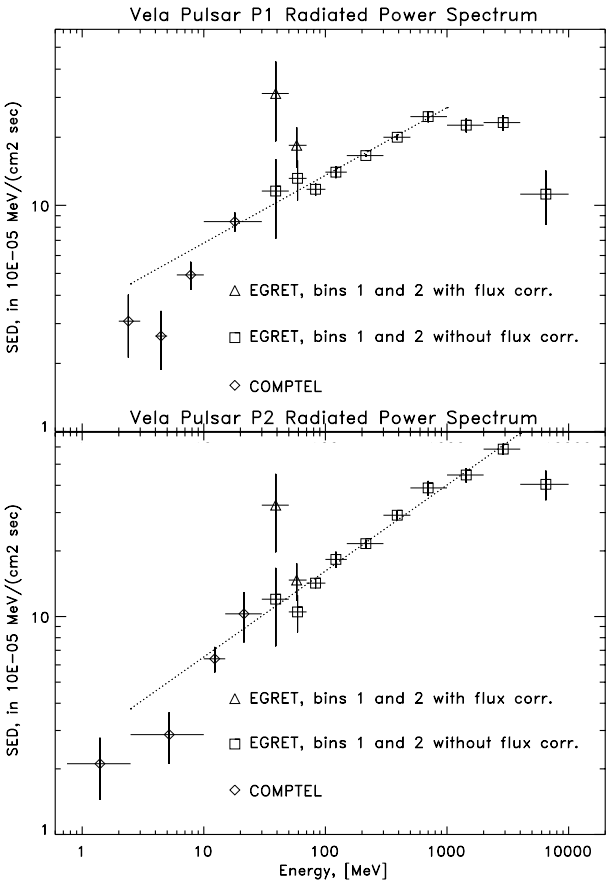

Fig. 5. Pulsed Vela pulsar spectra for phases P1 (upper plot) and P2 (lower plot) derived by using timing analysis for COMPTEL (Kuiper et al. 1998) and EGRET data (Fierro et al. 1998), covering observations of Vela pulsar during the whole CGRO mission.

These factors were introduced to correct for the apparent "flux deficit" in the two lowest energy bins of the Crab Nebula spectrum, an effect that we propose to explain by the giant dipole resonance absorption of photons in the Crab pulsar environment, i.e. an effect that is internal to the Crab Nebula emission region (Atoyan & Aharonian 1996; Komissarov & Lyubarsky 2003). The $\Delta\chi^2$ value for the Crab Nebula spectra (Fig. 6) is highly dependent on the model function used in the fit, and can be as small as that found for Geminga, but again the $\Delta\chi^2$ has the same negative sign; e.g. the quality of the fit improves after removing the flux correction coefficients for two lowest EGRET energy bins.

4. EGRET and COMPTEL spectra of QSOs

Until now, analysis of the recorded γ-ray spectra from different astrophysical objects, such as QSOs, pulsars, SNRs, binary systems, etc., were performed assuming that the spectrum emitted by the astrophysical object is typically smooth, even if the spectra are expected to have different shapes (power-law slopes) in different energy intervals. This also implies that the recorded spectra have to be smooth as well. This notion was used in a few cases for the in-flight calibration of the high-energy γ-telescopes as for EGRET (Thompson et al. 1993a; Esposito et al. 1999).

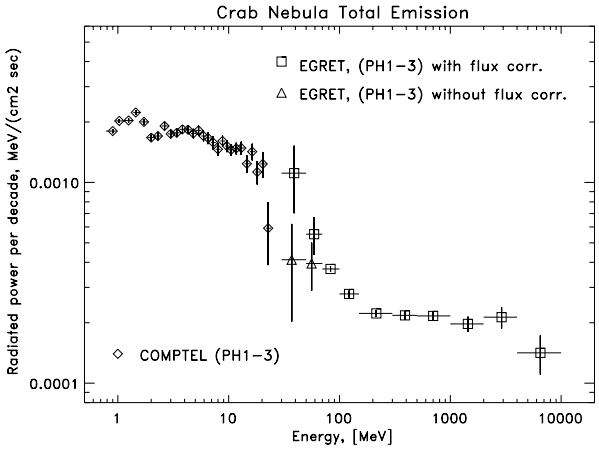

Fig. 6. Total Crab Nebula spectrum with small energy bins derived by using maximum-likelihood method for COMPTEL (van der Meulen et al. 1998) and by spatial analysis of EGRET data (Fierro et al. 1998), covering observations of Crab Nebula from 10 May 1991 till 4 October 1994.

Of course, an inter-instrumental calibration that assumes a smooth spectral match makes sense in view of the limited sensitivity of the gamma-ray telescopes employed to date. This limited sensitivity leads to few photon statistics collected for the single target during a reasonably short exposure, which has to be short because of the early apprehended variability of many sources of gamma-rays like AGN, X-ray transients, gamma-ray bursts, or solar flares. In reality, the differential photon flux from AGN detectable at the Earth can be written as a function of the photon energy and of redshift:

$$\frac{\mathrm{d}N}{\mathrm{d}E} = \left(\frac{\mathrm{d}N}{\mathrm{d}E}\right)_{\text{unabsorbed}} \cdot \mathrm{e}^{-\tau(E,z)}. \tag{2}$$

The dependence of τ on E and z, however, is quite complex and cannot be cast in a simple analytical expression.

To the first order of magnitude, though, we assume that we are dealing with absorbers at two redshifts, one in the QSO host galaxy and the second absorber in the Milky Way. This assumption is supported by our fitting results for SEDs of the γ-ray bright QSOs (see below Sects. 4.2, 4.3, 4.4, and 6.3) and is consistent with having minimally two concentrations of matter on the line of sight.

In analysing EGRET and COMPTEL spectra we used our own analysis results for the reprocessed data (Figs. 6–11), as well as published spectra of EGRET for QSOs (Figs. 12–18) that we converted into SEDs. Note that the brightness of these QSOs in the GeV energy domain may differ from their relative brightness in the MeV energy domain. Our results are presented as a set of contemporaneously measured, time-averaged, and flare spectra in the form of a spectral energy distribution (SED) for the QSOs 3C 273, 3C 279, PKS 0528+134, and BL Lacertae, which we will consider below.

4.1. Fitting procedure

Before proceeding with the description of the fit procedure, we note that all upper limits in SEDs of the QSO for the fitting purposes were converted into flux values that can be written as $\mathrm{SED}_{u.l.} = 1\sigma \pm 1\sigma$. In the fitting procedure we used the following routine.

As a first step, we fit a smooth function to the spectrum, that we choose to be the so-called "Band"-function (Band et al. 1993),

$$N_E(E) = A\left(\frac{E}{100\ \mathrm{keV}}\right)^{\alpha} \exp\left(-\frac{E}{E_0}\right), \tag{3}$$

$$\text{for} \quad (\alpha-\beta)E_0 \geq E, \tag{4}$$

$$N_E(E) = A\left[\frac{(\alpha-\beta)E_0}{100\ \mathrm{keV}}\right]^{\alpha-\beta} \exp(\beta-\alpha)\left(\frac{E}{100\ \mathrm{keV}}\right)^{\beta}, \tag{5}$$

$$\text{for} \quad (\alpha-\beta)E_0 \leq E. \tag{6}$$

This is capable of describing not only power-law spectra, but also spectra with a break. In the first fit of this smooth function to the SED, we do not include energy bins in the fit, which we believe do belong to the suspected troughs, in order not to bias the outcome. In this way we produce the simplest possible model to describe a specific SED. After selecting the initial fit parameters of the "Band"-function, α, β, E_0, and A, in the second fit we use energy bins of the SED that were used in the first fit, plus additional energy bins covering the suspected trough. In this second fit we use the sum of the "Band"-function and a Gaussian as a fit function, which means that we add another three free parameters to the fit function, namely the mean energy, the rms (σ), and the normalization of the Gaussian. Note that the number of fitted bins is also increased by the number of bins that belong to the fitted trough. From this fit we derive the value of $\chi^2_{\text{band+Gauss}}$ as a quality descriptor of the SED fit by the more complex model.

We then compare the value of $\chi^2_{\text{band+Gauss}}$ with the value of χ^2_{band} that we derive by the fitting again (third fit) the plain "Band"-function with the parameters derived from the first fit to the SED with the energy bins of the second fit, making sure that we are using exactly the same bins for the second and third fits. From second and third fits we derive the difference $\Delta\chi^2$, e.g., an improvement to the fit due to the addition of the Gaussian to the "Band"-function. We then evaluate the significance of this fit improvement by evaluating the probability of a spurious improvement of the fit from the value of $\Delta\chi^2$ for 3 d.o.f. as a test for such an improvement. In this test we follow Freeman et al. (1999), where the broader approach to statistical tests of both the simplest and more complicated models was discussed. We note that we do not constrain the fit parameters of the Gaussian describing an absorption trough co-added to the "Band"-function. Parameters resulting from fitting the SED of QSOs, including χ^2_{band}, $\chi^2_{\text{band+Gauss}}$ and $\Delta\chi^2$, are presented in Table 1, along with the probability of the spurious fit improvement, P_{spurious}. One may consider the inverse value of P_{spurious} as the significance of the fit improvement by applying a more complicated model (continuum function plus absorption feature described by a Gaussian) to the particular SED.

Table 2 provides values for the absorption trough position, which are given as E_1 for the Δ-resonance related trough, and E_2 as the GDR related trough. The width of these troughs

Table 1. Fits parameters of the QSO spectra and their significance.

Object	Observation	Absorption	$\chi^2_{\rm band}$	$\chi^2_{\rm band+Gauss}$	$\Delta\chi^2$	$P_{\rm spurious}$
3C 279	June 1991	GDR	72.0	35.9	36.1	6.2×10^{-8}
3C 279	June 1991	Δ	72.0	52.3	19.6	2.0×10^{-4}
3C 279	Feb. 1996	Δ	401.4	85.8	315.1	$<10^{-56}$
3C 279	Feb. 1996	GDR	401.4	145.8	255.5	$<10^{-45}$
3C 279	Jan. 1996	Δ	19.6	2.3	17.3	7×10^{-4}
3C 279	Time avrg.	Δ	157.9	61.5	96.3	2×10^{-20}
3C 279	Time avrg.	GDR	157.9	92.5	67.3	$\approx10^{-14}$
3C 273	Time avrg.	GDR	90.2	30.3	59.8	6×10^{-13}
PKS 0528	Mar. 1993	Δ	27.0	7.1	19.9	1.8×10^{-4}
PKS 0528	Mar. 1993	GDR	27.0	22.5	4.5	2.0×10^{-1}
PKS 0528	Time avrg.	GDR	48.3	25.4	12.9	5.0×10^{-3}
BL Lac	July 1997	Δ	55.3	31.6	23.7	3×10^{-5}

Table 2. QSOs and their absorption lines.

Object	Observ. time	$E_1 \pm \Delta E_1$	$z \pm \Delta z$	$\Delta F_1/F_1$	$E_2 \pm \Delta E_2$	$\Delta F_2/F_2$
		MeV		%	MeV	%
3C 279	June 1991	225 ± 75	$0.44(4) \pm 0.33(3)$	28 ± 14	24 ± 11	68 ± 11
3C 279	Feb. 1996	203.6 ± 6.6	0.596 ± 0.032	50–80	21.7 ± 5.4	74 ± 9
3C 279	Jan. 1996	207.5 ± 24.9	0.566 ± 0.12	46 ± 15	NA	NA
3C 279	Phase I–IV	192.6 ± 9.9	0.687 ± 0.051	$\sim$40	42 ± 13	93 ± 14
PKS 0528	Time avrg.	–	–	–	28.2 ± 4.8	57 ± 15
PKS 0528	Mar. 1993	105.95 ± 49.37	2.08 ± 0.47	34 ± 20	31.4 ± 13.8	60 ± 25
3C 273	Time avrg.	–	–	–	23.1 ± 4.1	50 ± 5
3C 273	Oct.–Nov. 1993	–	–	–	22.18 ± 10.06	28 ± 20
BL Lac	July 1997	278^{+63}_{-87}	$0.17^{+0.53}_{-0.22}$	40 ± 20	NA	NA

are not included in Table 2, but we have verified that the fitted Δ-resonance related trough width is consistent with the trough position and/or with the object redshift. Table 2 also presents the relative strength of the trough that we define as the ratio of (i) the peak value of the depression in the continuum, due to the Δ- or giant dipole resonance absorption; to (ii) the continuum fit above the trough. Values of F_1 and ΔF_1 describe the Δ-resonance trough continuum fit value and the flux depression at the Δ-resonance energy. In the same way F_2 and ΔF_2 describe the GDR trough continuum fitted flux and the flux depression at the GDR energy, respectively. Ratios of the ΔF_1 to the F_1, as well as ratios of $\Delta F_2/F_2$, can be used to estimate the column density of the absorber in the QSO environment or locally in the galactic halo and in the galactic disk.

To represent resonant absorption one can employ also the multiplicative profile

$$e^{(-\tau\cdot\exp(-(E-E_r)^2/2\sigma^2))},$$

where E_r is the centroid, σ the line rms, and τ the optical depth. Early work on the cyclotron absorption lines in spectra of Her X-1, for example, also began with additive and subtractive forms to represent line emission (see discussion in Gruber et al. 2001). For the GDR a Lorentzian profile can be also employed:

$$e^{(-\tau\cdot(\sigma\cdot E/E_r)/((E-E_r)^2+\sigma^2)},$$

with τ, E_r and σ as above. Generally, the optical depth τ is a function of photon energy and of the absorber redshift. In the simplest case absorption at a particular resonance can happen at the redshift of the host galaxy, as well as at redshift zero, i.e. in the halo or disk of the Milky Way. In a more complicated case, one may observe the QSO through the number of absorbers that are having different redshifts. To decompose such a complicated absorption pattern of troughs one would need plenty of photons and adequate energy and angular resolution for the γ-ray telescope.

Below we report results obtained by using a Gaussian energy dependence of optical depth at GDR and Δ-resonance, derived with the use of subtractive profiles. For the cases of two γ-ray bright sources 3C 279 and PKS 0528+134 we will show a difference in appearances of SEDs produced by either using or not using the flux correction coefficients (f.c.c.) of EGRET (Thompson et al. 1993a).

4.2. 3C 279

The optically violent variable (OVV) quasar 3C 279, also known as 4C 05.55, NRAO 413, and PKS 1253-05, is quite famous because of its luminosity variations in the optical (Pica et al. 1988), radio, and X-ray bands (Aller et al. 1985; Zamorani et al. 1984; Webb et al. 1990; Wehrle et al. 2001;

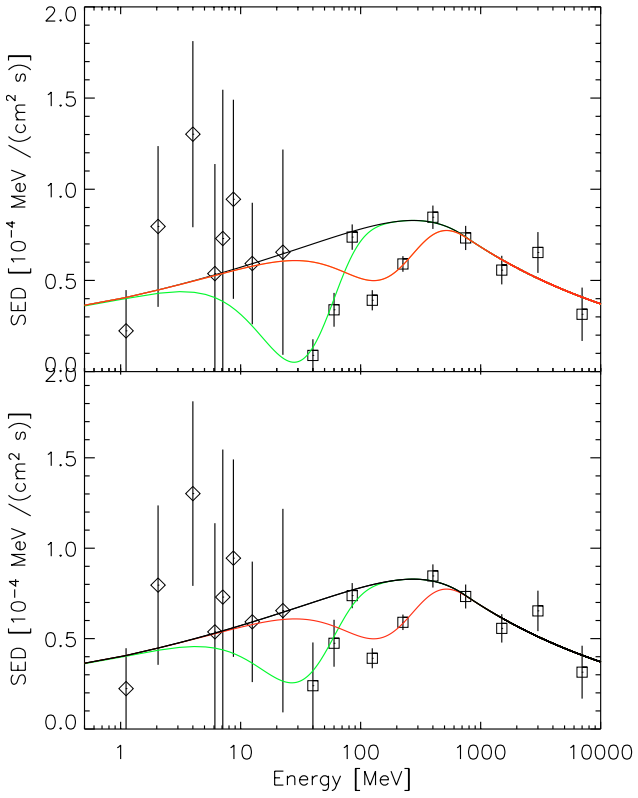

Fig. 7. *Upper*: a plot of the 3C 279 time-averaged SED measured during CGRO Phases I–IV (1991-1997), produced without using the EGRET flux correction coefficients. It includes fits of the Δ resonance photon absorption in the QSO environment (red line) and of the GDR resonance photon absorption in the local galactic environment (galactic halo) shown by a solid green line. A black line shows "Band"-function fit to the SED. *Bottom*: the same as the upper plot, but for the SED produced with the use of EGRET flux correction coefficients. Diamonds show COMPTEL derived spectral points, and boxes mark EGRET spectral points.

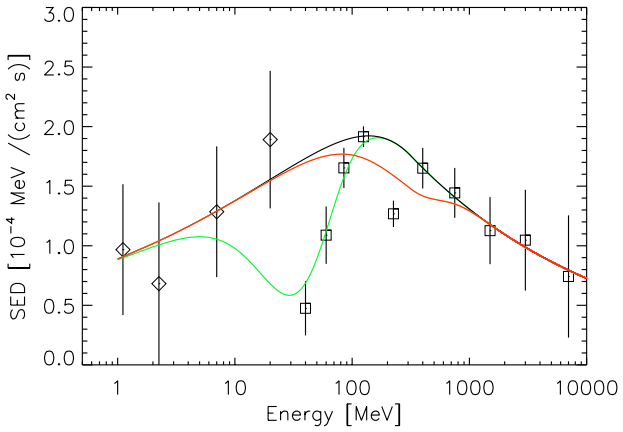

Fig. 8. A fit to the 3C 279 spectral energy distribution measured during CGRO viewing periods VP003.0 and VP 011.0, that includes the Δ resonance photon absorption in the QSO environment (red line), and the GDR resonance photon absorption in the local galactic environment (galactic halo) shown by green line. Diamonds and boxes are used as in Fig. 7.

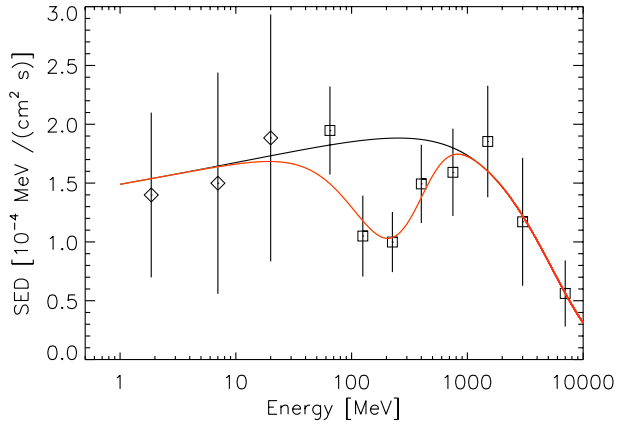

Fig. 9. A fit to the 3C 279 power spectrum measured during the flare of January 1996, which includes the Δ resonance photon absorption in the QSO circumnuclear environment. Line colours, diamonds, and boxes have the same meaning as in Fig. 7.

Ballo et al. 2002). The activity of 3C 279, which is one of the brightest γ-ray QSOs in the EGRET energy range, was monitored by γ-ray telescopes on board CGRO (Hartman et al. 1999). Because of 3C 279 brightness in the EGRET energy range it is one of the best candidates to confirm our findings on the Δ-resonance absorption in the rest frame of the flaring QSO. Figure 7 presents the 3C 279 time-averaged spectrum, contemporaneously measured by COMPTEL and EGRET, with the GDR resonance fit to all data points of the SED that is shown by the green line and the Δ-resonance fit as shown by the red line, respectively. Figures 8–10 show spectra for three active phases of the QSO 3C 279. We have plotted low energy points of EGRET spectra omitting the flux correction introduced by the EGRET Team (Thompson et al. 1993b) (upper plot) and using the flux correction coefficients (lower plot). We notice that all spectra of 3C 279, time-averaged (Fig. 7), or flare spectra (Figs. 8, 10) show notable absorption features. Only one spectrum from a January 1996 flare does not show a prominent GDR absorption trough because three low energy bins of EGRET, namely 30–50 MeV, 50–70 MeV, and 70–100 MeV were combined into one energy bin of 30–100 MeV in this particular case (Fig. 9), which precludes any statement about the presence of an absorption trough in the GDR energy range for this individual flare period of QSO, while the trough around 200 MeV of the EGRET energy interval for 3C 279 is seen in all spectra (Figs. 7–10).

Thus, the Δ-resonance related trough is clearly present in the time-averaged SED of 3C 279 (Fig. 7), as well as in SEDs measured during strong flaring episodes of 3C 279 in June 1991 (Fig. 8), January 1996 (Fig. 9) and February 1996 (Fig. 10). It is important for the case of photo-absorptions seen at the GDR energies that the 3C 279 flare spectra also definitely contain the GDR trough (Fig. 7, lower plot) even if the depth of the trough is slightly smaller than that for the upper plot of Fig. 7.

To derive position and strength of the trough we used the three-step approach to the spectrum fit as described in Sect. 3.1. From the measured SEDs of 3C 279 one can derive the weighted mean energy of the Δ-resonance trough in the observer coordinate system as $E_{\Delta}^{\rm measured} = 203.5 \pm 3.5$ MeV. By using the known redshift of 3C 279 we re-calculate the trough

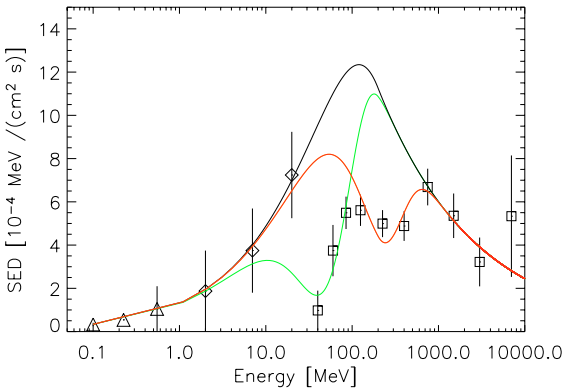

Fig. 10. A fit to the 3C 279 spectral energy distribution measured during the flare of February 1996, which includes the Δ resonance absorption feature produced in the QSO environment (red line) and the GDR resonance absorption feature (green line) produced in the low redshift local environment (galactic halo). Diamonds and boxes have the same meaning as in Fig. 7, and triangles show OSSE spectral points from Collmar (2003).

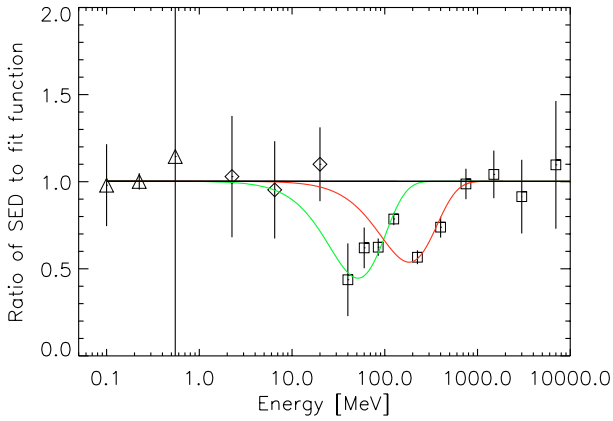

Fig. 11. A fit to the weighted mean of the ratios of the 3C 279 three flares SEDs. The ratios were derived in the two-step procedure: first SEDs (with the f.c.c. used) were fitted with a "Band"-function, to which ratios of the SEDs were derived in the second step for QSO flares of June 1991, January 1996, and February 1996. From these individual ratios a weighted sum was produced. The fit contains a GDR resonance absorption feature (green line) produced in the low redshift local environment (galactic halo) and also includes the Δ resonance absorption features at the redshifts of the QSO host galaxy and of the Milky Way, as shown by the red line. The black line shows the normalised ratio of the SED to the "Band"-function fit without absorption. Diamonds and boxes have the same meaning as in Fig. 7, and triangles show OSSE points from a paper by Collmar (2003).

energy in the QSO rest frame as $E_{\Delta}^{\rm restframe} = 313 \pm 10$ MeV. This is remarkably close to the expected value of the peak position in the absorption cross section at the Δ-isobar resonance.

Moreover, Figs. 7, 8, and 10 of the time-averaged and flare spectra of 3C 279 indicate another trough at energies ∼23 MeV. We note that Figs. 8 and 10 were produced without using the flux correction coefficients (see below Fig. 11 with the use of f.c.c.).

The trough at ∼23 MeV corresponds to the peak position of the giant dipole resonance (GDR) that is produced by photon absorption on the different elements in the absorbing matter. We note in passing that the GDR absorption trough shape is dependent on the metallicity of the absorbing matter. It is important for the general case of photo-absorption that 3C 279 time-averaged and flare spectra are definitely contain the GDR trough independently of the f.c.c. application. This is clearly supported by the plots of Fig. 7 for the time-averaged SED of 3C 279, and of Fig. 11, where the weihted mean of ratios of three individual flare SEDs of 3C 279 (with f.c.c. applied) to their appropriate fits is shown.

4.3. 3C 273

3C 273 ($l = 289.95°$, $b = 64.36°$, $z_{\rm QSO} = 0.158$) is one of the brightest quasars in the sky at X- and γ-ray wavelengths. It has been frequently observed with COMPTEL and EGRET (Lichti et al. 1995; von Montigny et al. 1997), as well as by OSSE (McNaron-Brown et al. 1995) on board CGRO. It is also one of the best studied directions in the sky in the UV, optical, and X-ray wavelength ranges (Courvoisier 1998; Türler et al. 1999). 3C 273 has a superluminal, strongly variable jet with many knots that are produced during different QSO outbursts (Sambruna et al. 2001; Marscher et al. 2002; Jorstad & Marscher 2003).

The most surprising feature of the time-averaged γ-ray spectrum of 3C 273 (Fig. 2, 12) is the ∼7 MeV trough. Figure 12 also clearly points to the presence of another trough in the SED of 3C 273, namely at $E_\gamma \sim 25$ MeV. Again, in order to derive the trough position and strength we have used the three-step approach to spectrum fit as described in Sect. 3.1.

Figure 12 shows a fit to the time-averaged SED of 3C 273 in the region of the GDR resonance absorption, while Fig. 13 shows the SED of the 3C 273 flare in October–November 1993 with a fit to the 3C 273 SED in the Δ resonance region. Results of the fit to the time-averaged SED of 3C 273, including the GDR absorption trough, are presented in Table 2. The absorption fit in Fig. 13, as shown by the red line, is based on one bin of the flux depression in the SED, which is not enough to obtain a convincing fit of the trough at ∼300 MeV. But curiously, the energy of the trough derived from the 3C 273 SED of Oct.–Nov. 1993 is consistent with the Δ resonance, even if the position is derived with ∼100% error.

4.4. PKS 0528+134

The next QSO studied within the framework of this photon absorption technique is PKS 0528+134. It was observed regularly by CGRO because of its relative proximity to the Crab Nebula, which was a calibration source for EGRET, as well as due to its flaring activity in X-rays and in EGRET energy range (Thompson et al. 1993b; Mukherjee et al. 1996; Collmar et al. 1997; Mukherjee et al. 1999). Figure 14 presents the time-averaged SED of PKS 0528+134, covering CGRO Phases I–IV for EGRET (Mukherjee et al. 1999) and Phases I–III for COMPTEL data (Collmar et al. 1997), fitted with the "Band"-function plus one Gaussian to describe the GDR resonance absorption trough. Note that the 10–30 MeV flux measurement of COMPTEL in the SED of PKS 0528+134 does not have a

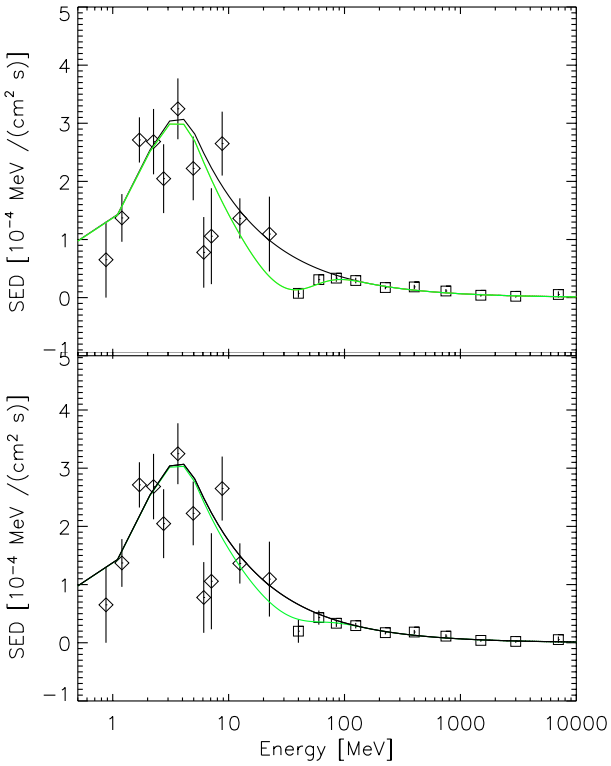

Fig. 12. *Upper*: A plot of the 3C 273 time-averaged SED measured during CGRO Phases I–IV (1991–1997), which was produced without the EGRET flux correction coefficients. It includes fit of the GDR resonance photon absorption in the local galactic environment (galactic halo) shown by the green solid line. Black line shows "Band"-function fit to the SED. *Bottom*: The same as the upper plot, but for the SED produced with the use of EGRET flux correction coefficients. Diamonds and boxes have the same meaning as in Fig. 7.

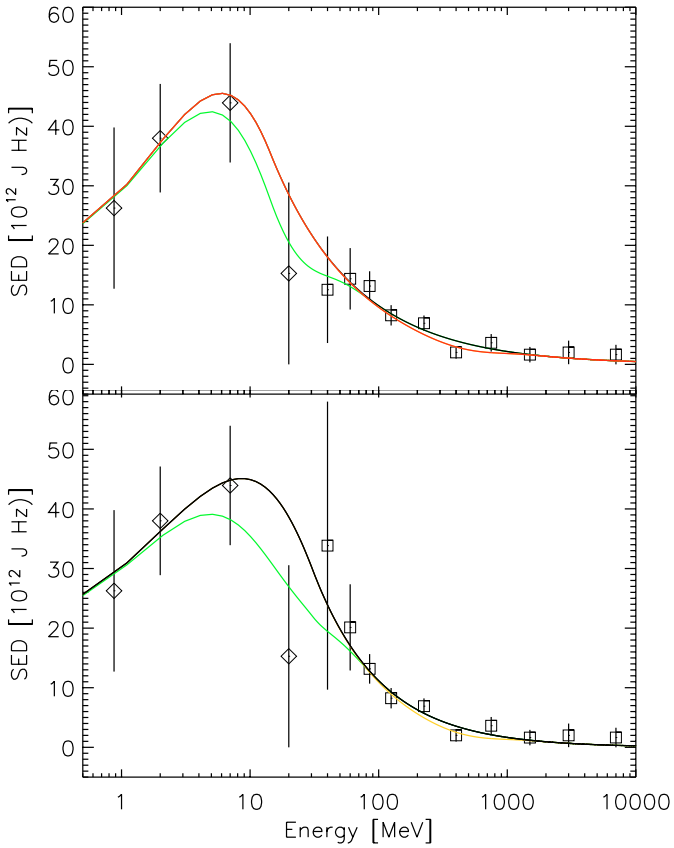

Fig. 13. *Upper*: A plot of the 3C 273 SED measured during the flare of October–November 1993 and produced without using the EGRET flux correction coefficients. It includes fit of the GDR resonance photon absorption in the local galactic environment (galactic halo) shown by the green solid line and the Δ-resonance fit shown by the red line. A black line shows "Band"-function fit to the SED. *Bottom*: The same as upper plot, but for the SED produced with the use of EGRET flux correction coefficients. Diamonds and boxes have the same meaning as in Fig. 7.

strong influence on the fit. This is not a surprise considering the low significance (~2.3σ) of the COMPTEL 10–30 MeV flux measurement. The more significant lowest energy bins of EGRET define the SED fit at γ-ray energies from 10 MeV to 100 MeV.

Similarly to Fig. 14, Fig. 15 shows the SED of PKS 0528+134 measured during the QSO flare in March 1993 (VP 0213.0). Again, one can easily spot the trough related to the GDR absorption resonance, while the flux depression related to the Δ resonance is depicted by only one bin at 100–150 MeV. Other fitting parameters of PKS 0528+134 troughs are presented in Tables 1 and 2.

To judge the influence of the EGRET f.c.c. use on the amplitude of the absorption troughs we show one more spectrum of PKS 0528+134. One of them is the QSO flare SED normalised to the "Band"-function fit of the PKS 0528+134 for the PKS 0528+134 flare during observation VP000.0, and the second spectrum is a weighted sum of the ratios of three flares of PKS 0528+134 of VP000.0, VP001.0, and VP0213.0 to their appropriate "Band"-function fit (Fig. 17). Note that the GDR trough is clearly observed in all three figures, Figs. 15–17. At the same time we note that the higher-energy trough of Fig. 16 can be fitted assuming two absorbers on the sight line. One

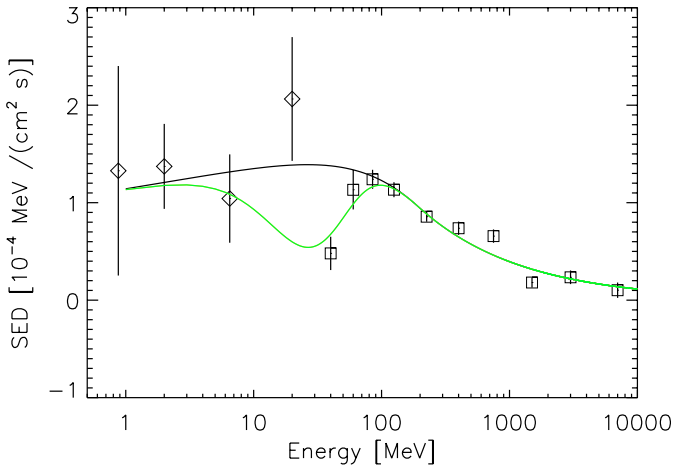

Fig. 14. A fit to the PKS 0528+134 time-averaged SED derived by using the maximum-likelihood method for EGRET data during CGRO Phases I–IV (Mukherjee et al. 1999) and for COMPTEL data (from Collmar et al. 1997) covering observations of PKS 0528+134 during CGRO Phases I–III, which includes the GDR resonance photon absorption in the local galactic environment (galactic halo). Diamonds and boxes have the same meaning as in Fig. 7.

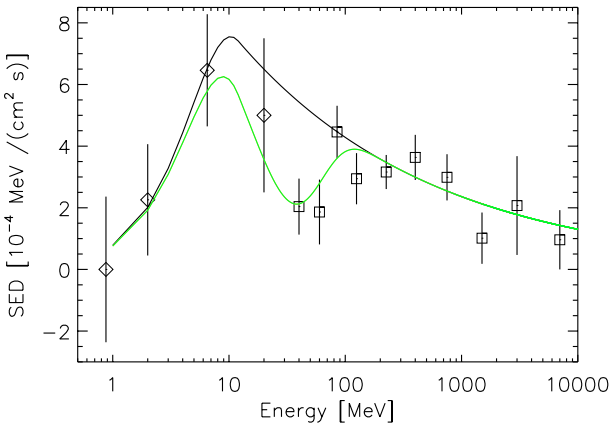

Fig. 15. The SED of PKS 0528+134 measured during CGRO observation 0213.0 (Collmar et al. 1997; Mukherjee et al. 1999) and fitted with a function that includes the GDR resonance photon absorption in the local galactic environment. Line colours, diamonds and boxes have the same meaning as in Fig. 7.

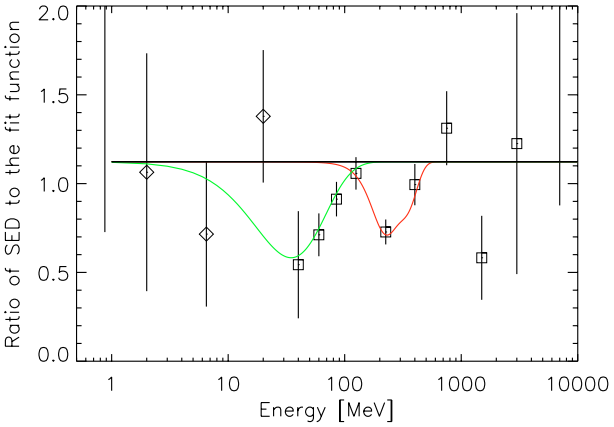

Fig. 16. The SED of PKS 0528+134 measured for the strongest flare of the QSO during the CGRO observation VP000.0 (Thompson et al. 1993a), normalised to the "Band"-fit function (black line) and then fitted with a function that includes the GDR resonance photon absorption in the local galactic environment (green line). A red line gives an impression of the possible two absorbers fit to the SED. These two absorbers are at $z_1 \sim 0$ and $z_2 \sim 0.5$. Diamonds and boxes have the same meaning as in Fig. 7.

absorber is asssumed to be at $z = 0$, i.e. in the Milky Way, and the second absorber is placed at the redshift of $z < 2$.

4.5. BL Lacertae

BL Lacertae is another bright QSO at a redshift of $z = 0.069$. BL Lac objects have been interpreted as extreme cases of a beamed source in which the Doppler boost is so large that a substantial portion of the observed optical spectrum is dominated by nonthermal emission from the jet (Blandford & Königl 1979). BL Lac was first detected at energies >100 MeV by EGRET in 1995 (Catanese et al. 1997). In July 1997, during an optical flare of BL Lac, it was again significantly detected by EGRET (Bloom et al. 1997; Böttcher & Bloom 2000) and by X-ray telescopes (Madejski et al. 1999; Grove & Johnson 1997; Ravasio et al. 2003). During this flare the spectrum of

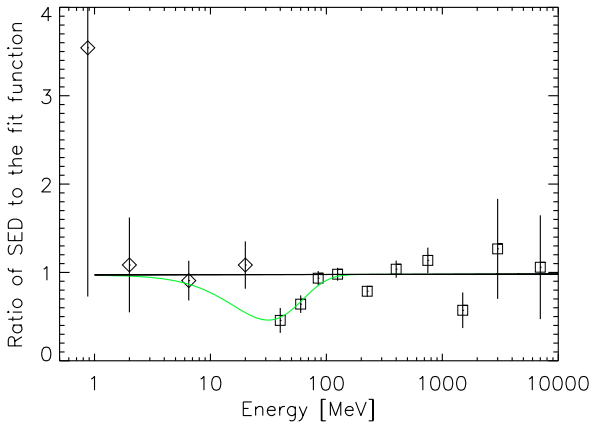

Fig. 17. The weighted mean ratio of the PKS 0528+134 SEDs to their appropriate fit functions derived forflares during observations VP000.0 (Thompson et al. 1993a), VP001.0 (Collmar et al. 1997), and VP0213.0 (Mukherjee et al. 1999). The mean ratio was fitted with a function that includes the GDR resonance photon absorption in the local galactic environment (green line). Diamonds and boxes have the same meaning as in Fig. 7.

BL Lac was significantly harder compared to the time-averaged spectrum of 3EG J2202+4217 (Hartman et al. 1999). This hard spectrum provided us with enough statistics to fit a Δ-resonance absorption trough to its SED of July 1997. Figure 18 shows the resulting fit, and Table 1 contains the values of χ^2_1, χ^2_2, and $\Delta\chi^2$ to allow us to judge the fit quality, while Table 2 provides information on the energy of the fitted trough. The redshift value of $z \sim 0.17^{+0.5}_{-0.2}$ for BL Lac, which was derived from the July 1997 flare SED by our absorption method, is a rather crude estimate, but it is broadly consistent with the optically measured redshift of $z = 0.069$.

Several measurements of the X-ray spectrum in the 2–300 keV energy range were performed for BL Lac by OSSE (Grove & Johnson 1997), RXTE (Madejski et al. 1999), and Beppo-*SAX* (Ravasio et al. 2003). Spectral coverage of the BL Lac July 1997 flare was good enough to note the change of the dominant emission mechanism of BL Lac from synchrotron self-compton (SSC) at low X-ray energies, to the external photons Compton up-scattering (EC) as the dominant emission mechanism at $E_x > 300$ keV (Sambruna et al. 1999). Detection of the Δ-resonance trough in BL Lac during its flare state points to the presence of a jet or of an accretion disk wind in the system during periods of an influx of gas into circumnuclear region of the AGN. This might explain the detection of strong emission lines from BL Lac on a few occasions (Corbett et al. 1996), and it effectively supports an idea of the stengthening of the ionizing radiation source that is likely associated with the accretion disk (Corbett et al. 1996) in the BL Lac type of AGN.

5. Identification of some EUIDs

The introduced γ-quanta absorption technique can be used for the evaluation of the absorbing column in the cases of QSOs with the known redshift. At the same time the approach can be reversed and used to evaluate the redshift of objects of

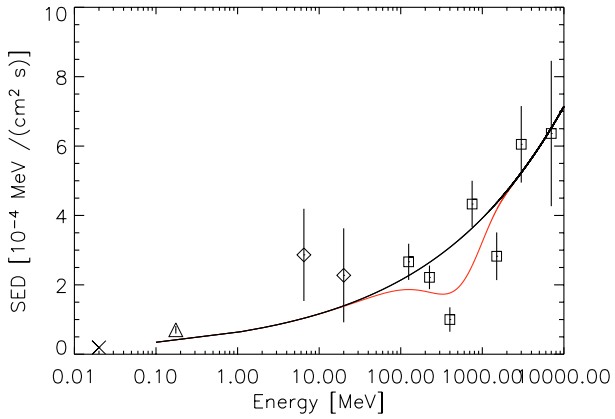

Fig. 18. A fit to the BL Lacertae spectral energy distribution of the July 1997 flare by the fit function that includes the Δ resonance photon absorption in the circum-QSO environment (red line). A cross shows the SED fit value from the RXTE PCA measurements at 20 keV (Madejski et al. 1999), and a triangle shows OSSE measured flux in 50–300 keV energy interval for this flare (Grove & Johnson 1997). Diamonds are COMPTEL measured fluxes and boxes are EGRET measurements for the BL Lac July 1997 flare. A black line is the "Band"-function fit.

unknown identification (EUID). For this purpose we selected a few sufficiently bright EUIDs (Hartman et al. 1999) and analysed their SEDs.

Indeed, from the Δ-resonance trough measurements of 3C 279 we derived the "γ-measured" averaged redshift of 3C 279 as $z = 0.60 \pm 0.02$ (see redshifts for 3C 279 in Table 2). We note that the systematic shift of the through position to lower energies (higher redshift) is explained by the relative decrease in the SED point density with the γ-ray energy in EGRET spectral analysis. Namely, we have ~5.7/dex points for $E_\gamma \leq 100$ MeV, 4/dex points for 100 MeV $\leq E_\gamma \leq 1000$ MeV, and 3/dex points of SED for $E_\gamma \geq 1000$ MeV. The bin density per decade of energy is important for the fitting of a complex model, like a "Band"-function plus a Gaussian to the SED. This systematic shift can be calibrated for a given binning of the SEDs. The precision with which the redshift value (z) determined using this procedure may be as high as $\Delta z \sim 0.1$ or better, subject to the object's γ-ray brightness and position of the trough in the energy range of the γ-ray telescope used to produce SED.

For our small sample of EUIDs, we derived parameters of the high-energy troughs, and from their position evaluated a plausible redshift that is needed to explain the trough shift to the lower energies in the observer frame. The results of this approach are quite encouraging. In Table 3 we present values of the χ^2 derived by the EUID SED fitting with the "Band"-function, as well as with the combination of the "Band"-function and one Gaussian. A note of caution: The number of free parameters while fitting a combination of "Band"-function and of Gaussian to the EGRET only SED is usually ≤3, which is rather small for a good fit, especially when the position of the suspected trough overlaps, or is close to the position of the break energy of the "Band"-function fit.

5.1. 3EG J1744-3011

This is an example of the case where application of the EGRET f.c.c. is of no importance for the fit, and a seemingly significant and convincing fit of the "Band"-function plus Gaussian (see Table 3 and Fig. 19) was produced. Visually, from the SED shape (Fig. 19), it is clear that the position of the trough is consistent with ~350 MeV; i.e. 3EG J1744-3011 does not have any significant redshift and can equally well be a galactic source or an extragalactic source at the redshift of ~0. Indeed, from the fit we got the energy of the high-energy trough (Δ-resonance) at $E_1 = 420^{+42}_{-75}$ MeV, which is consistent with the source being galactic and effectively has zero redshift that can be formally derived as $z \pm \Delta z = -0.23^{+0.18}_{-0.07}$.

Precision of the redshift estimate for this EUID can be improved by using more data points, including those of COMPTEL. Unfortunately, the angular resolution of COMPTEL does not allow the 3EG J1744-3011 ($l = 358.85°$, $b = -0.52°$, with 0.32° radius of 95% error contour) to be clearly separated from the excess that is associated with the stronger EGRET source 3EG J1746-2851.

5.2. 3EG J1746-2851

This unidentified source was detected by EGRET from the direction towards Galactic Center (GC) (Mayer-Hasselwander et al. 1998). This region, which contains Sgr A$*$ as its dynamical center with the black hole of an estimated mass of 4×10^6 $M_\odot$, was observed in a wide range of wavelengths (Sofue et al. 1986; Pedlar et al. 1989; Koyama et al. 1996; Purcell et al. 1997; Maeda et al. 2002; Tsuchiya et al. 2004). The GC contains a strong, variable radio (Zhao et al. 2003) and weak, but occasionally flaring infrared (Genzel et al. 2003) and X-ray (Baganoff et al. 2001) source.

The bright 3EG J1746-2851 source is listed as unidentified in the third EGRET catalog (Hartman et al. 1999) at the galactic position of $l = 0.11°$, $b = -0.04°$, which is consistent with the GC position that is within a 95% confidence contour radius (0.13°) of 3EG J1746-2851. It has been considered as the γ-ray counterpart to GC (Mayer-Hasselwander et al. 1998) with different scenarios of the γ-ray production, like inverse Compton radiation from relativistic electrons from one or a few of the filamentary structures near the GC, or even as a Cold Dark Matter (CDM) annihilation result,or combined emission of a few pulsars in the region. Indeed, N-body simulations suggest significant enhancement of the CDM density around galaxy cores (Navarro et al. 1996). Other alternative scenarios include γ-ray emission arising from the decay of neutral pions, which were produced by high-energy protons accelerated in the assumed SNR, interacting with the ambient matter (Fatuzzo & Melia 2003). Time variability of 3EG J1746-2851 reported by Nolan et al. (2003), though, makes a few of the above scenarios untenable.

We have re-analysed the SED of 3EG J1746-2851 by combining the EGRET spectrum of the source with the EGRET f.c.c. applied with the COMPTEL spectral points (Figs. 20, 21). Applying the photon absorption method to the SED of 3EG J1746-2851 led to significant fit improvements by

Table 3. EUID, their absorption lines, and redshifts derived from the fit.

Object	$\chi^2_{\rm band}$	$\chi^2_{\rm band+Gauss}$	$\Delta\chi^2$	$P_{\rm spurious}$	$E_1 \pm \Delta E_1$	$z \pm \Delta z$
3EG J1744-3011	26.7	6.6	20.1	1.7×10^{-4}	420^{+42}_{-75}	$-0.23^{+0.18}_{-0.067}$
3EG J1746-2851	304.3	37.3	266.9	$<10^{-40}$	177.8 ± 26.6	0.83 ± 0.15
3EG J2016+3657	46.6	31.8	14.8	$\sim 2 \times 10^{-3}$	91.53 ± 13.25	2.55 ± 0.15
3EG J2016+3657*	90.8	9.7	81.0	2.3×10^{-17}	$130.04^{+6.8}_{-7.0}$	$1.50^{+0.14}_{-0.13}$

* For the case of SED with the use of the f.c.c. of EGRET.

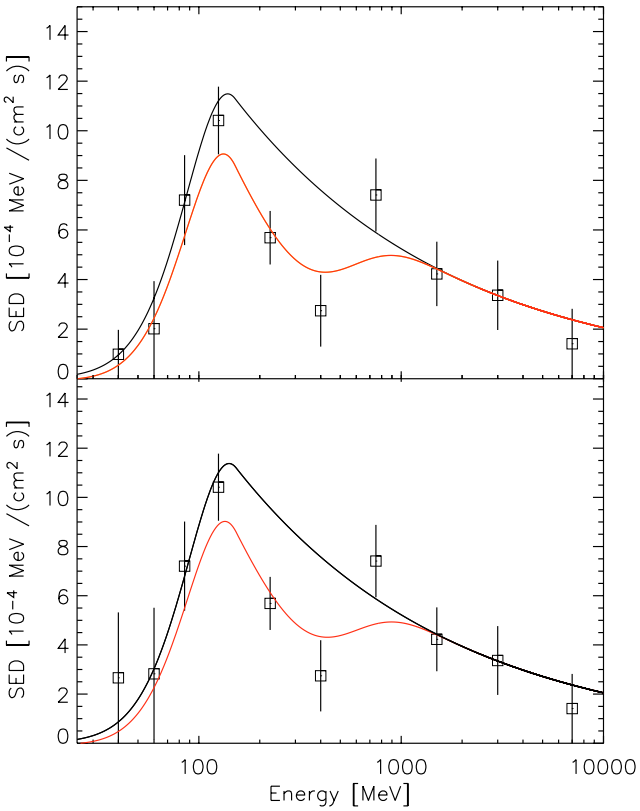

Fig. 19. *Upper:* a plot of the 3EG J1744-3011 time-averaged SED measured during CGRO Phases I–IV (1991–1997), which was produced without using the EGRET flux correction coefficients. It includes the fit of Δ-resonance photon absorption (red line). Black line shows "Band"-function fit to the SED. *Bottom*: the same as the upper plot, but for the SED produced with the use of EGRET flux correction coefficients. Boxes show EGRET spectral points.

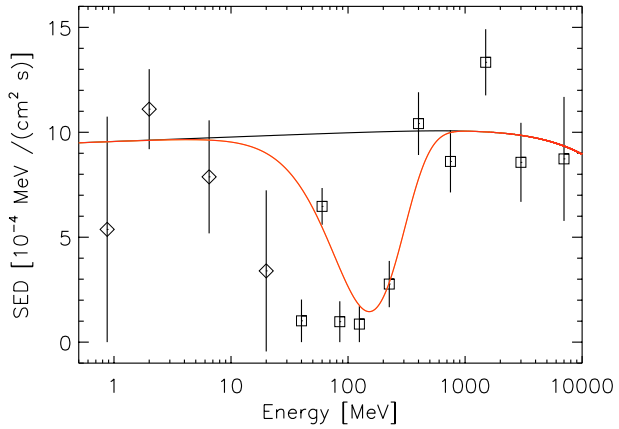

Fig. 20. A fit to the 3EG J1746-2851 spectral energy distribution that includes the Δ resonance photon absorption in the circum-QSO environment. Line colours, diamonds and boxes have the same meaning as in Fig. 7.

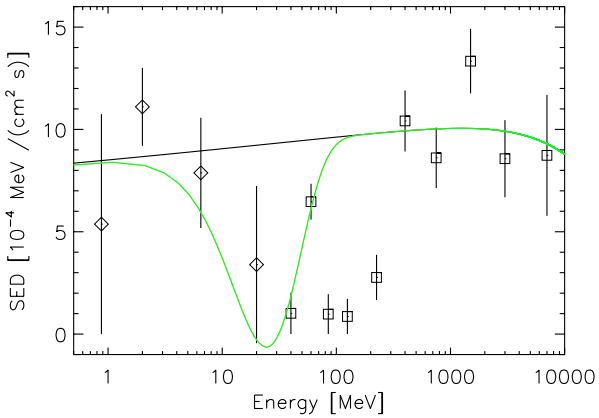

Fig. 21. A fit to the 3EG J1746-2851 spectral energy distribution that includes giant dipole resonance photon absorption along the path that goes through the galactic center environment, which is optically thick even for the MeV γ-rays. Line colours, diamonds and boxes have the same meaning as in Fig. 7.

comparing it to the fit with a smooth "Band"-function. Both troughs at $E_\gamma \sim 20$ MeV and at ~150 MeV are highly significant (see Table 3), but positions of both troughs are very dependent on the detection significance of the EGRET fluxes at 30–50 MeV, and 50–70 MeV. If we do not take these two low energy bins at 30–50 MeV and 50–70 MeV into fit, then we derive an energy of 177.84 ± 26.6 MeV for the Δ-resonance related trough of 3EG J1746-2851 and a redshift of the probable counterpart, namely of the QSO behind the Milky Way Galactic Center, as $z = 0.83 \pm 0.15$. If we include both low energy bins into fit of the Δ-resonance trough, then we get even higher redshift of the source 3EG J1746-2851, namely $z = 1.08 \pm 0.12$, for $E_1 = 156 \pm 19$ MeV. This result we consider as a strong hint of an alternative interpretation of the γ-ray emission from the GC direction which underlines the need for a deeper search of the GC region for other than galactic contributors.

Quite interestingly, CANGAROO-II (Tsuchiya et al. 2004) and HESS (Aharonian et al. 2004) have recently announced the significant, but spectrally disparate detection of sub-TeV γ-ray emission from a position consistent with the 3EG J1746-2851. This detection may play an important role in identifying 3EG J1746-2851 as an extragalactic blazar, rather than the interpretation favoured by both teams, e.g. that of the GC origin of the sub-TeV and GeV γ-ray emission from this direction.

For the GDR related trough of 3EG J1746-2851 we found an energy of $E_2 = 25.7 \pm 1.8$ MeV or, equivalently, the redshift of the absorber of $z = 0.02 \pm 0.07$. Poor statistical significances of the COMPTEL spectral points do not allow any conclusion on the presence or absence of the GDR-related trough in the absorber with the redshift consistent with that derived from the fit to Δ-resonance related trough. The depth of the GDR related trough of 3EG J1746-2851 is readily explained by an absorber in our galaxy, namely by the bulge matter that is concentrated towards GC. In this region the mean density of the gas is expected to be as high as $\sim 10^3$–10^4 cm^{-3} (Maeda et al. 2002) on the scale of a few kpc, e.g. along the galactic bulge major axis. If we take the size of the bulge's major axes as ~5 kpc, as was suggested by Freudenreich (1998), we derive a column density towards 3EG J1746-2851 of $\geq 10^{26}$ cm^{-2}. A similar value is also needed to explain large GDR absorption for 3EG J1744-3011, which is most likely located somewhere behind the Milky Way.

Results of the SED fitting of 3EG J1746-2851, as well as of 3EG J1744-3011 are strongly dependent on the galactic diffuse model used in extracting the appropriate SED. A better model of the galactic diffuse γ-ray emission will be needed to finally clarify the origins of 3EG J1746-2851 and of very high energy γ-ray emission from the GC direction.

5.3. 3EG J2016+3657

Mukherjee et al. (2000) discuss this unidentified EGRET source with the galactic coordinates $l = 74.76°$ and $b = 0.98°$, and with 0.55° radius of 95% position error contour. Considering results of the multiwavelength behavior of the probable candidate, it was concluded that a blazar type source behind the galactic plane is the most probable counterpart for this EGRET source.

Our results from fits to the SED of this source are in line with such an interpretation on the probable counterpart of 3EG J2016+ 3657 (see also Halpern et al. 2001). We found that the most likely source has a redshift of ~1.5–2.55, which follows from the fit of the Δ-resonance trough in SED of this source (Fig. 22, Table 3). We believe that this redshift will help to plan follow-up observations of the plausible counterpart at this high redshift.

6. Discussion

Quasars are among the most luminous AGN in the Universe and thus visible out to very high redshifts. The multitude of AGN, which are powered by the accretion of gas onto an SMBH located at the centers of galaxies at redshifts $z \sim 2$–3, indicates an epoch of BH growth. It is also an epoch of strong star formation in young galaxies. The evolutions of the total star formation rate of the Universe and the space density of luminous quasars appear to be very similar. Both show a strong increase of more than an order of magnitude from $z = 0$ to $z = 2$. Beyond this redshift the number density of quasars again drops, suggesting that $z \sim 2$ is the epoch when the majority of spheroidal galaxies in the Universe was forming.

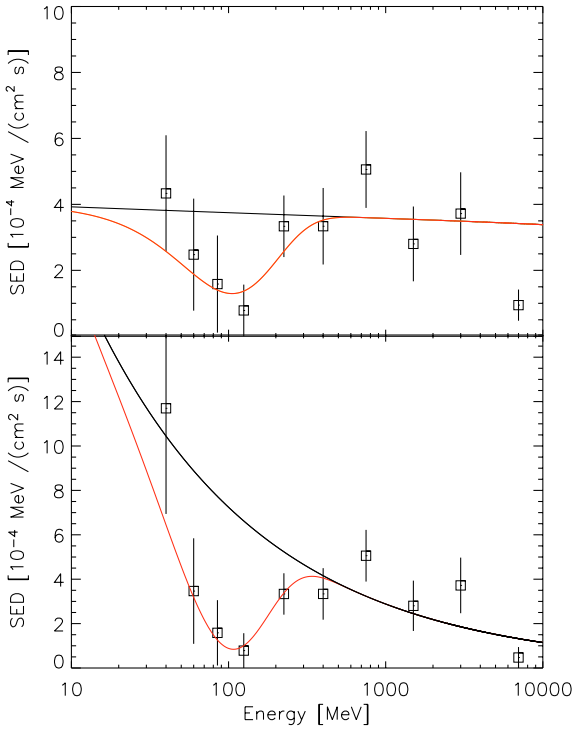

Fig. 22. *Upper*: a fit to the 3EG J2016+3657 SED produced without using f.c.c., which includes the Δ resonance photon absorption in the circum-QSO environment. *Below*: the same but for the SED produced using f.c.c.. Line colours and boxes have the same meaning as in Fig. 7.

Surveys of galaxies in infrared and sub-millimeter wavelengths have revealed a substantial number of high-redshift sources where the star formation rate exceeds 1000 solar masses per year, enough to create a massive galaxy in only a small fraction of the Hubble time. Such coeval star formation was detected in a good fraction of luminous high-redshift quasars (Carilli et al. 2001; Omont et al. 2001).

Recent submillimeter observations of X-ray absorbed and unabsorbed AGN with $z \sim 1$–3 seem to support an evolutionary scenario for the MBH growth. Strong submillimeter emission at 850 μm, an isotropic signature of copious star formation, was found only in the X-ray absorbed sample of AGN, ruling out orientation effects as the cause of the absorption (Page et al. 2004). These observations support the idea that substantial absorption in AGN could be a definite characteristic of the early phases of QSO evolution (Fabian 1999). In such a model, the main obscured growth phase of the QSO coincides with formation of the host galaxy spheroid, the completion of which indicates the beginning of the luminous, unobscured phase of the QSO's evolution (Silk & Rees 1998).

Understanding the co-evolution of galaxies and black holes requires knowledge of the accretion history of MBH, which can be acquired by studying so-called "type 2 QSOs", e.g., heavily absorbed AGN. Up to now very few "type 2 QSO" have been found (Norman et al. 2002; Stern et al. 2002; Dawson et al. 2003). Of course, UV-excess or optical surveys would not have found most obscured AGN, nor would soft X-ray surveys such as the ROSAT All-Sky Survey (Voges et al. 1999).

QSO flaring activity, as well as the steady emission from QSOs during their obscured evolution, contribute to the Cosmic X-ray Background (CXRB),which has been resolved in the 0.5–5 keV band and found to consist mostly of both unabsorbed and absorbed AGN with column densities $<10^{23}$ cm^{-2}. This contrasts with the local AGN population where the column density range extends to Compton-thick objects and beyond ($>1.5 \times 10^{24}$ cm^{-2}). Stacking analysis of the integrated emission of sources detected by XMM-Newton in the Lockman Hole and by Chandra in the CDF-N and S reveals that the resolved fraction of the X-ray Background drops above 6 keV and is about 50% above 8 keV. The missing flux has the spectrum of a highly absorbed AGN, making it likely that the range of column density at redshift one is similar to that locally and that many AGN are as yet undetected in well-studied fields (Fabian 2004).

That obscured AGN are common is obvious from the fact that the three nearest AGN with intrinsic X-ray luminosities above 10^{40} erg/s (NGC 4945, the Circinus galaxy, and Centaurus A) are all highly obscured with $N_{\rm H} > 10^{23}$ cm^{-2} (Matt et al. 2000). Two (NGC 4945 and Circinus) are even Compton-thick with $N_{\rm H} > 1.5 \times 10^{24}$ cm^{-2}. This situation has only been slowly appreciated, perhaps because NGC 4945 appears as a starburst galaxy at all non-X-ray wavelengths and because the Circinus galaxy lies close to the Galactic plane. The background spectrum in the 2–10 keV band is flatter than typical AGN and requires that most are absorbed (Setti & Rees 1989; Madau et al. 1994; Comastri et al. 1995). This ties in with what we know of AGN locally, where absorbed Seyfert II galaxies outnumber Seyfert Is. At greater distances where higher luminosity objects are sampled, there are some clear highly absorbed AGN (e.g., NGC 6240, Vignati et al. 1999; IRAS 09014, Iwasawa et al. 2001; 3C 294 nucleus, Fabian et al. 2003). In particular, the nuclei of many radio galaxies lie behind large column densities.

Distant obscured AGN (redshift $z > 0.3$) are now being found in large numbers by X-ray observations with *Chandra* and *XMM-Newton* (Mushotzky et al. 2000; Alexander et al. 2001; Barger et al. 2001; Brandt et al. 2001; Crawford et al. 2001; Giacconi et al. 2001; Hasinger et al. 2001; Rosati et al. 2002). Most of the serendipitous sources found in an X-ray image above 1 keV made with these telescopes are obscured. Source variability in many cases makes an AGN identification unambiguous. The determination of column densities requires that the source is identified and its redshift known. Hence, the redshift determination is now possible with the γ-ray absorption method.

6.1. Absorption column densities

Observations at different wavelengths probe different depths of the AGN environment. Under the assumption of a Galactic gas-to-dust ratio in the circum-nuclear matter of AGN, a V-band extinction of $A_V = 1$ mag corresponds to a column of neutral hydrogen $N_{{\rm H},z} \sim 1.5 \times 10^{21}$ cm^{-2}. Thus for the extinction of $A_V < 5$ the broad-line region in AGN can be observed. Beginning with $A_{\rm V} \sim 5$–8 the broad optical lines are unobservable, but still AGN can be identified by observations in the Paschen series of lines in the infrared regime (IR). For higher extinctions one has to progressively use longer wavelength lines like Paβ (λ1.2818 μm) for $A_V \leq 11$, whereas for extinctions up to $A_V \approx 26$ one will already need to use Brγ (λ 2.1655 μm) and finally Brα (λ 4.0512 μm) that can probe up to $A_V \approx 68$ (Veilleux et al. 1997). For extinction values $\geq$100 γ-ray observations have to be performed to provide a direct view of the central engine of AGN. We note that for $A_V > 500$, or equivalently at $N_{\rm H} > 10^{25}$ cm^{-2}, the AGN nucleus is hidden even for 10 keV photons. Such opaque matter is optically thick to Compton scattering, and the central source is only detectable via scattering by material out of the line of sight. In cases like that even the AGN classification strongly depends on the wavelength at which it is observed, which can potentially lead to confusion in questions of the source's nature.

Reliable measurements of the absorption column densities in the troughs are crucial for determining the energetics, abundances, and ionization distribution in the outflows and in the intervening absorbers. The early phases of the obscured AGN evolution and of BH growth are heavily obscured in X-rays, optical, and UV. These phases are only observable in far-infrared (sub-millimeter), or even better in penetrating γ-rays. A few recent studies of absorption features in the SEDs of AGN (Arav 1997; Barlow 1997; Telfer et al. 1998; Arav et al. 1999; Churchill et al. 1999; Ganguly et al. 1999; de Kool et al. 2001; Arav et al. 2002) have demonstrated that in quasar outflows most absorption lines are saturated even when not black, and the column densities inferred from the depths of the troughs are only lower limits.

In the X-ray, as well as in the γ-ray regimes, the apparent optical depths can be expressed in the same way as in the optical or UV band, while using a cross section to quantify the probability of the γ-ray interaction (absorption) process (see Appendix). From the ratio of typical absorption cross sections in the γ-ray and X-ray regimes it follows that troughs detected in γ-rays will deliver information on the column density on the order of ${\sigma_\Delta}^{-1}$, for the Δ-resonance trough, or on the order of ${\sigma_{\rm GDR}}^{-1}$ for the giant dipole resonance absorption, while in the X-ray regime a Thompson cross section $\sigma_{\rm T}$ has to be used to evaluate an absorption in X-rays. To quantify these ratios we use values of $\sigma_{\rm T} \sim 0.7$ barn, $\sigma_\Delta \sim 0.5$ mb, and $\sigma_{\rm GDR} \sim 3.6$ mb. That means that we can probe the optical depth of the QSO environment up to $N_{\rm H}$ values of $\sim 2 \times 10^{27}$ cm^{-2} via the Δ-resonance absorption of γ-rays, while in the X-ray regime we are limited to column densities on the order of 10^{25} cm^{-2}. The lower limit of the column density that can be tested via the γ-ray absorption method is dependent on the statistics of the particular measurement, which, in turn, is dependent on the sensitivity of the γ-ray telescope, on the source brightness in the γ-ray band, and the source exposure.

The important factor that may influence determination of the absorbing column densities is the possibility of multiple-scattering, which can eventually lead to the smearing of the trough due to the scattering of the higher-energy photons in the energy window of a resonance. This may happen via Compton scattering or via the cascading of high-energy photons to the energy window of the appropriate resonance trough. This

problem is not a new one, as the same kind of difficulty was encountered while measurements of the total photon attenuation coefficient were being performed (Conner et al. 1970; Hubbell 1971; Varier et al. 1986). To completely solve this problem one has to iteratively simulate the propagation of the photon spectrum through the matter by using the derived column density to evaluate the effect of re-scattering of the narrow beam of photons on the observable SED. This work is in progress, and the results will be published elsewhere (Iyudin et al. 2005).

There is a way out, though, that can help to ease the problem of this re-scattering; namely, assuming (i) that the transverse dimension of the absorber is less than ∼5 attenuation lengths at the energy of the highest attenuation value (Varier et al. 1986) or (ii) that the absorber consists of many clumps (clouds) of matter with 5–10 clouds typically on the line of sight helps to minimize re-filling of the absorption troughs. This geometry is similar to the one used to describe the optically thick absorbers around QSO central engines in UV, X-ray (Arav et al. 2003, 2005) and IR (Elitzur et al. 2003). For the solar mixture of absorber the minimal attenuation length in the energy range we discuss is ∼86 g cm^{-2} or, alternatively, $\sim 5 \times 10^{25}$ cm^{-2}. Therefore, for an absorber with the thickness of less than 2.5×10^{26} cm^{-2} in the direction transverse to the photon beam (line of sight), the process of photon re-scattering into the beam is expected not to be of a large influence. The total smearing (filling) effect is expected to be ≤10% of the SED value in the trough.

In the first approximation we assume that the photon spectrum produced along the jet has to pass through a medium with a column density of D (cm^{-2}), which we take to be uniform in the sense of a fixed metallicity in the QSO host galaxy along the line of sight. If the cross section of the photon absorption process is described by $\sigma(E)$, dependent only on photon energy in the rest frame of the QSO, then we have a transmission law of the QSO emission through this matter similar to Eq. (2) (see Sect. 3), where an exponential describes the transmitted part of the photon flux from the QSO for photons of energy E. Here we assume that $\mathrm{d}N/\mathrm{d}E_{\mathrm{unabsorbed}}$ represents a spectrum that is completely formed and decoupled from the bulk motion of the jet. The absorber column density is then equal to the integral of the target nuclei number per unit volume n along the physical extension of the absorber slab Δr, e.g., along the observer's line of sight.

Equation (2) is a simplified representation of the complex transformation of the SED after decoupling from the jet on its way from the emission region towards the observer. In the first approximation we neglected the effect of comptonization on the SED, which leads to a shift of the luminosity to lower energies, as well as to the effect of cascading. The Comptonization of the SED is usually invoked for photon energies $E_\gamma \leq \epsilon_{\mathrm{cr}}$, where ϵ_{cr} is the characteristic energy of the absorber. For photons with $E_\gamma \geq \epsilon_{\mathrm{cr}}$ a diffusion equation has to be used, to properly describe the transfer and evolution of the SED due to cascading in the thick absorber (see Aharonyan & Plyasheshnikov 2003, and below Sect. 5.5).

By definition the integral of the absorbing column (D) along the line of sight is proportional to the N_{H}, which is a standard quotation in X-ray and optical absorption studies. Here, N_{H} is a column density of hydrogen atoms along the line of sight from the observer to the emitting source (QSO). In our simplified case $N_{\mathrm{H}} = n_{\mathrm{H}} \times \Delta r$, for a constant density of the target nuclei along the line of sight. We can rewrite the above transmission expression as follows:

$$F_{\mathrm{Obs}}(E) = F_0(E)\left[\exp\left(-\sigma_{\mathrm{eff}} N_{\mathrm{H}}^{\Delta r}\right)\right], \tag{7}$$

where we have used a σ_{eff} derived for the specified metallicity, for example a solar metallicity of the absorbing slab. For such a mixture of elements in the absorber the effective Δ-resonance absorption will occur on all elements of the mixture, and an absorption cross section has the form of

$$\sigma(E) = \sigma_{\mathrm{H}}(E) + \sum_i \sigma_i(E) f_i, \tag{8}$$

while for the GDR absorption cross section the effective cross section will be defined by photon interactions on all elements heavier than hydrogen, mainly by ^{4}He

$$\sigma(E) = \sum_i \sigma_i(E) f_i. \tag{9}$$

Here, σ_i is the cross section of an element (isotope) i, and f_i is the number abundance of the ith element relative to hydrogen. We take the solar composition by mass (number of nucleons) where hydrogen composes ∼71% of all the gas mass, helium ∼27%, and all other heavy elements only 1.9% of the total gas mass.

To derive the value of $\Delta F_j/F_j$, where j takes the values of 1 or 2 as in Table 2, we use Eq. (7) from which follows

$$\frac{\Delta F_j}{F_j} = \left[1 - \exp\left(-\sigma_{\mathrm{eff}} N_{\mathrm{H}}^{\Delta r}\right)\right], \tag{10}$$

where Δr is the total geometrical thickness of the absorber along the sight line from the observer to the γ-ray source, and the column density $N_{\mathrm{H}}^{\Delta r}$ is integrated along this sight line. Note that the real geometry of the absorber in the circumnuclear region of QSO and/or generally in the QSO host galaxy can be quite different from the simplified picture of a homogenous slab. An absorber between the QSO central engine and the observer more likely consists of many clouds that differ in their density, temperature, and element mixture. Such absorbers consisting of many clouds can have a covering factor anywhere between 0 and 1. This complication is ignored at the moment.

6.2. Origin of observed troughs

The QSO γ-ray emission spectrum is believed to form quite near the black hole, independently of the blazar emission mechanism, whether "proton"-like (Mannheim 1993; Mücke et al. 2003), or "electron"-like (Blandford & Königl 1979; Burns & Lovelace 1982). The emission spectrum forms at typical distances $\gtrsim 10^3$ Schwarzschild radii (r_{s}) from the BH. At smaller distances from the BH the cooling time of electrons, as well as protons, near the base of a jet is very short, because it is governed by photon cooling (Dermer & Schlickeiser 1994). This cooling will lead to a prominent spectral "bump" at soft X-ray energies due to Comptonization of external UV photons

by cold electrons in a jet, but such "bumps" have not been observed.

The lack of such features in the observed SEDs indicates that acceleration and collimation of the jet takes place at rather large distances from the supermassive BH. The bulk motion of the jet will slow down at the radial distances $r \gtrsim 10^{18}$ cm (Celotti et al. 1998; Blandford 2000; Georganopulos & Kazanas 2004), e.g. at a distance from the BH that is associated with the broad line emission or with absorption regions (BLR, or BALR) in quasars. At such large radial distances from the BH, the γ-ray spectrum can be considered as already formed.

The shape of the γ-ray spectrum, decoupled from the jet bulk motion, will be further governed by the photon-matter interaction with the host galaxy matter. For the high-energy γ-quanta these interactions are important already at the circum-QSO optical depth on the order of $\tau \geq 1$ radiation length, e.g. $\geq$86 g/cm^2. This value of the absorbing column is about equal to the unit of radiation length for the solar composition of the matter in the QSO host galaxy, and is smaller than the absorption column values derived from the observed absorption troughs in SED of γ-ray loud QSOs.

Possible constituents of the absorbing matter in QSOs can be thought of as an optically thick jet/wind loaded with baryons observed at a small angle to the jet axis and/or as clumps (clouds) of cold matter crossing the line of sight from the massive black hole towards an observer that are placed somewhere near the jet lobe, or just outside of the jet, i.e. in the cocoon of the jet.

Winds heavily loaded with matter were observed by XMM-Newton from the quasars PG 1211+143 (Pounds et al. 2003) and PDS 456 (Reeves et al. 2003). King & Pounds (2003) have shown that black holes accreting near or above the Eddington rate are capable of producing optically thick winds. This result implies that in QSOs accreting at or close to the Eddington rate (>0.1 $\dot{M}_{\rm Edd}$), gamma-rays with energy of $E_\gamma > 100$ MeV will interact with the material of the wind, and further out with the host galaxy matter on their way towards the observer.

In the sufficiently thick layer of such matter γ-rays will experience not only resonant absorption, which we have discussed above, but also multiple interactions with the baryonic matter, leading finally to the development of electron-photon shower, similar to the cascade well known from the study of high-energy cosmic rays (Rossi & Greisen 1941; Aharonian & Plyasheshnikov 2003). The spectra of γ-rays finally escaping from such optically thick environment will typically have a power law shape with a photon index of ~2.0 and a high energy cut-off at $E_\gamma \sim$ few GeV.

The cut-off energy in QSO spectra may vary from one flare to another for the same QSO, but all spectra will have a typical roll-over at energies exceeding a critical energy ($\epsilon_{\rm cr}$), if the object is observed along the sight line that is close to the jet axis through the obscuring matter with a thickness $\geq$1 radiation length (Rossi & Greisen 1941; Aharonian & Plyasheshnikov 2003). Therefore we conclude that the observed troughs in the SEDs of QSOs can be produced, at least in part, by the interaction of the γ-ray beam, formed quite near BH, with the QSO circumnuclear matter, as well as with the host galaxy bulge and/or halo matter.

Clearly one always needs a sufficiently bright source for an absorption study in the selected waveband. The same condition applies to the present study of absorbers in the QSO environment, where we have used the brightest known QSOs in the MeV and 100 MeV to 10 GeV energy range. These QSOs are quite well studied at other wavelengths, so that we know their geometry to some degree. In outflow geometry like that in radio-loud QSOs with the jet opening angle taken according to the radio measurements (Jorstad & Marscher 2003), we are observing the QSO's central engine along the line of sight and through the matter that was expelled with the jet(s) and that remains entangled by the jet for the duration of the QSO flare.

Using Eq. (10) we derive $\Delta F_j/F_j$ as given in Table 2. It is clear that we are probing column densities on the order of 10^{27} cm^{-2} and 10^{26} cm^{-2} in cases of Δ-resonance absorption and GDR absorption, respectively. For example, one can derive a column density of $N_{\rm H}^{\rm GDR} \cong 8.1 \times 10^{26}$ cm^{-2} for the ratio of $\Delta F_2/F_2 \sim 0.6$ and $N_{\rm H}^{\Delta} \cong 6.9 \times 10^{26}$ cm^{-2} for the ratio of $\Delta F_1/F_1 \sim 0.3$, in the cases of the 3C 279 flare SED of 1991 and of the PKS 0528+0134 flare SED of March 1993, respectively (see Table 2).

Celotti et al. (1998) evaluated typical values for the densities of clouds in the jet at different radial distances from the BH. For a typical luminosity of the QSO jet of $L_{\rm jet} \sim 10^{46}$ erg s^{-1}, Celotti et al. (1998) have defined the parameter space of the cloud density against the radial distance of the cloud from BH, which leads to an integral absorption column value estimate on the order of a few 10^{23} cm^{-2} up to the distance of 10^{18} cm. The integral column density of the jet matter will vary from one to another QSO or even for different flares of the same QSO, but it is small to explain the observed Δ-resonance absorptions for different flares of QSOs, unless there is a region along the jet, up to the radio lobes, where all or part of the absorbing baryons are accumulated during the QSO evolution. We envisage the geometry of the cocoon extended along the QSO jet, which is similar to that proposed to explain both the free-free absorption in young radio galaxies (Bicknell et al. 1997; Begelman 1999) and an increase of the star formation activity in the host galaxies of high-luminosity AGN (Kauffmann et al. 2003).

If the Δ-resonance absorption is produced by the beam interaction with the matter in the halo of the host galaxy, then the amplitudes ($\Delta F_1/F_1$) of the Δ-resonance trough will be of comparable strength for different flares of the selected QSO. Similarly, the position and amplitude of the GDR-resonance absorption, measured in the rest frame of Milky Way, is expected to always be the same for the selected QSO, as seems to be the case for our small sample of QSOs (see Table 2 and Sect. 6.3).

6.3. Other expected troughs

The positions of the high energy troughs found in the gamma-ray spectra of four QSOs 3C 273, 3C 279, BL Lac, and PKS 0528+134 are consistent with the position of the Δ-isobar related resonance in the photon absorption cross section,

if presented in the QSO rest frame. We have used redshifts of $z = 0.158$ for 3C 273, $z = 0.536$ for 3C 279, $z = 0.069$ for BL Lac, and $z = 2.06$ for PKS 0528+134. The position and significance of the trough for 3C 279 is especially convincing (see Sect. 3.2). It means that we can use Δ-isobar trough position to verify the redshift of the known source (QSO), or to derive the redshift of the unidentified source from the appropriate SED.

The interpretation of the lower energy trough that we suggested is produced by the GDR type absorption is obviously not consistent with the QSO's rest frame. If we calculate a weighted mean value of the GDR related troughs from the spectra of our four QSOs, we derive a value of $\langle E \rangle_{\rm GDR} = 25.1 \pm 2.5$ MeV, which is consistent with the position of GDR absorption on ^{4}He (MacCormick et al. 1997) at the redshift $z \approx 0$. Indeed, for the solar composition of absorber, one expects to have a 14.2:1 ratio of the absorption on ^{4}He to that on other, heavier nuclei. Therefore, the GDR trough shape and position for the solar composition of the absorber are largely defined by the properties of the GDR of ^{4}He (see Fig. A.2).

Quite logically, after detecting a Δ-resonance trough in the SED of a particular QSO, one also expects to detect an even stronger GDR trough produced by the same absorber in the rest frame of QSO. In practice, for SEDs consisting of the combined EGRET and COMPTEL data, the GDR related trough will fall into the energy range of COMPTEL for all QSO with redshift >0. Unfortunately, for the sensitivity of COMPTEL the detection of such a redshifted GDR trough will be marginal as soon as the radiated energy density in the trough drops below 10^{-4} Mev^2 (cm^2 s MeV)$^{-1}$, which is the case even for the brightest in the MeV energy domain QSO, like 3C 273 (see Fig. 10). Therefore, all presented GDR trough detections at $E_\gamma \sim 20$ MeV are largely defined by EGRET fluxes in the 30–50 MeV and 50–70 MeV energy bins. We recall here that our analysis of SEDs was made by discarding use of the flux correction coefficients, which generally makes deeper GDR troughs. Our approach is also supported by the expected ratio of the GDR trough to that of the Δ-resonance absorption trough if produced by the same absorber (see below).

In relation to the detected GDR trough we recall here that the lines of sight toward 3C 273 and 3C 279 pass through the Radio Loop IV, where an excess absorption in O VI was observed by Savage et al. (2003). This line of sight crosses a bright soft X-ray filament near the edge of Radio Loop IV (Snowden et al. 1997). The region that is placed in projection between Loop I and Loop IV is also known to produce the so-called Extreme Scattering Events in the radio emission of the background QSOs (Fiedler et al. 1994).

Additionally, observations of 3C 273 by XMM-Newton (de Vries et al. 2003) and by *Chandra* (Fang et al. 2003) have lead both groups to claim an extra component in the X-ray absorption spectrum, which is identified as neutral oxygen. Our analysis of PV data for 3C 273 observations with XMM-Newton, revolution 0277, confirms presence of the absorption trough of a neutral O I in the 3C 273 spectrum at $\lambda \sim 23.4$ Å (see Fig. 23) in the RGS1,2 spectra. We note that O I absorption line strength is an order of magnitude higher than the O VII and O VIII absorption lines of 3C 273 (Fig. 24). These X-ray absorption features do not have a measurable

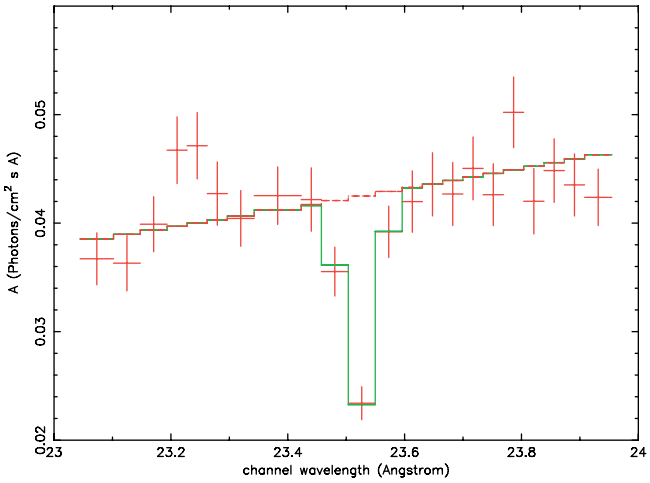

Fig. 23. X-ray absorption spectrum of 3C 273 for observation during the 277 revolution of XMM-Newton in the line of neutral oxygen (OI).

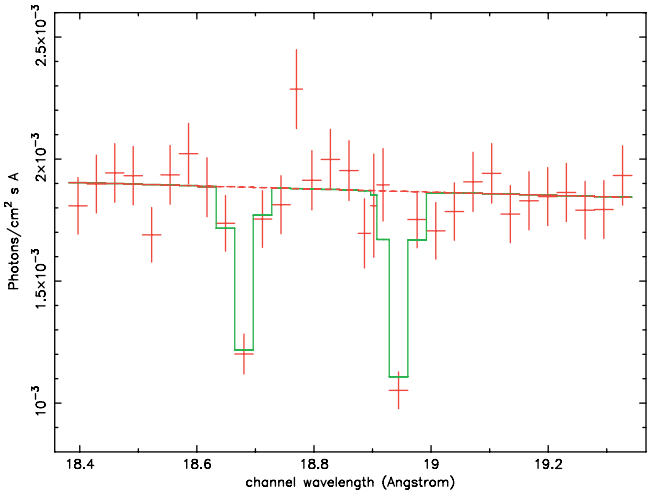

Fig. 24. X-ray absorption spectrum of 3C 273 for observation during the 277 revolution of XMM-Newton in the lines of OVII and OVIII.

redshift; therefore we conclude that they are related to the halo absorber component. The related trough may also be present in the γ-ray absorption spectra of 3C 273 and 3C 279. Therefore, we propose that the strong absorption trough at ~7 MeV in the 3C 273 time averaged spectrum of COMPTEL (Fig. 2), as well as the GDR troughs of 3C 273 and 3C 279 SEDs, can be explained by such a local galactic absorber.

If this is the case, then we should observe a broadening of the Δ-resonance related trough for 3C 279, which is bright at these energies. Indeed, an inspection of SEDs presented in Figs. 6–9 leads us to conclude that the *FWHM* of the high-energy trough, as featured in the time-averaged (Fig. 7) and in the flare SEDs (Figs. 8–10) of 3C 279, is clearly broader than for the expected *FWHM* of a single trough. The observed *FWHM* values exceed the expected *FWHM* for the Δ-resonance trough produced by the absorption in the 3C 279 rest frame ($z = 0.536$), e.g. the value of ~(160/1.536) MeV, which is ~100 MeV. We observe *FWHM* of the Δ-resonance trough of ~270 MeV for the 3C 279 flare of February 1996, and ~320 MeV for the 3C 279 flare of January 1996. Clearly, these

*FWHM*s exceed the expected width value by far for the single trough and are consistent with the presence of the blend of two troughs, one at $z = z_{\rm QSO}$ with the position of ~200 MeV and another at $z = 0$ with the position of 325 MeV.

The amplitude of the latter Δ-resonance trough, if decomposed from the sum of two troughs, can be used: first, to derive and compare an absorbing column with that of the GDR trough measured from the same SED at $z = 0$, and second, to make a sanity check by deriving the ratio of the GDR and of the Δ-resonance troughs, which has to be equal to the $\exp((\sigma_{\rm GDR} - \sigma_{\Delta})D)$, where D is the column density of the absorber. In the case of the time-averaged SED of 3C 279, the shape of the Δ-resonance trough is also consistent with such an interpretation.

A similar check will be possible to perform for any of the γ-ray bright QSOs or EUIDs, provided that the γ-ray data available for such a check has the sensitivity and energy resolution sufficient enough to have at least 7 or more energy bins with the significant flux measurements in the region of the high-energy troughs. For QSO at $z = 2.0$ it means that one will need to use a γ-spectrometer with an energy resolution of at least $\Delta E/E \leq 15\%$, which is within reach. See, for example, `http://www-glast.slac.stanford.edu` for the GLAST parameters and MEGA `http://www.mpe.mpg.de/gamma/instruments/mega/` for the medium energy telescope description and anticipated performance parameters.

6.4. X- and γ-ray derived absorption columns

Are absorption column values derived via gamma-ray absorption too high? To answer this question one can compare the above estimates of $N_{\rm H}$ for the circum-nuclear region of 3C 279 with values of $N_{\rm H} \geq 10^{25}$ cm^{-2}, which follow from the X-ray obscuration studies of AGN by Maiolino et al. (1998), Risaliti et al. (1999), Matt et al. (2003), and Comastri (2004).

As support for the measured gamma-ray absorption columns we may take the recent consensus that the absorbing column in AGN is variable and can be even larger than $N_{\rm H} \geq 10^{25}$ cm^{-2} (Risaliti et al. 2002; Matt et al. 2003; Comastri 2004). This is particularly promising, because high absorption column values were measured during times of the QSOs high flaring activity, i.e. during times when the new influx of accreted matter was falling into a potential well of the AGN black hole. More sensitive measurements of the QSO SEDs during their flares can help to understand where the absorbing baryonic matter is placed: in the jet itself, in the jet cocoon, or in the host galaxy halo.

There have been numerous attempts to account for the origin of the cosmic X-ray background (CXRB) with populations of active galactic nuclei (AGN) integrated over cosmic time (Setti & Woltjer 1989; Madau et al. 1994; Celotti et al. 1995; Comastri et al. 1995). In this case, Fabian & Iwasawa (1999) have recently shown that the CXRB sources plausibly account for all of the accretion power in the Universe and that most of it is intrinsically absorbed. We also note that the shape of the cosmic X-ray background spectrum (Gilli et al. 2001) seems to require introducing a strongly absorbed population of the AGN to explain the shift of the CXRB spectrum peak to X-ray energies of $E_{\rm x} \sim 30$ keV (Urry & Treister 2004). The baryonic matter content of the heavily absorbed population of AGN will be possible to probe with the γ-ray absorption method, thus providing the means to put the above hypothesis of the CXRB origin on firm grounds.

7. Summary

We have introduced a novel γ-ray absorption method based on the application of resonant absorption by nuclei of high energy photons, e.g. processes that are well known in nuclear physics. We demonstrate application of this method to known quasars, as well as to the bright γ-ray sources obviously obscured at other wavelengths (EUIDs). Unlike X-ray or UV-absorption studies, where the ionization state of the absorber is very important in the derivation of the absorbing column, the γ-ray absorption method is completely independent of the ionization and/or of the chemical state of the absorber.

Application of the γ-ray absorption method, already feasible for instruments with EGRET sensitivity, will be indispensable in studies of baryonic matter distribution in the Local Group galaxies by γ-ray telescopes like GLAST (see Iyudin et al. 2005). At the same time instruments with sufficient energy resolution and sensitivity in the MeV to 300 MeV energy range can provide information on the content and metallicity of the baryonic matter in the QSO host galaxy via detection of the redshifted troughs in the SED of QSOs, produced via the GDR and Δ-resonant absorption of γ-ray photons emitted by the QSO. It will be especially useful for studying AGN during their obscured evolutionary phase. This possibility arises due to the different contributions of hydrogen and of all other elements to the absorption in the GDR and nuclear resonance absorption region, if compared with that of the isobar resonance energy region.

Acknowledgements. This research has made use of the NASA/IPAC Extragalactic Database (NED) operated by the Jet Propulsion Laboratory, California Institute of Technology, under contract with the National Aeronautics and Space Administration, as well as of NASA's Astrophysics Data System Service. AFI acknowledges financial support from the BMBF through the DLR grant 50 OR 0002.

References

Aharonian, F. A., & Plyasheshnikov, A. V. 2003, APh, 19, 525
Aharonian, F. A., Akhperjanian, A. G., Barrio, J. A., et al. 2001, A&A, 366, 62
Aharonian, F. A., Akhperjanian, A. G., Ayer, K.-M., et al. 2004, A&A, 425, L13
Ahrens, J. 1985, Nucl. Phys. A, 446, 229c
Ahrens, J., Borchert, H., Czock, K. H., et al. 1975, Nucl. Phys. A, 251, 479
Ahrens, J., Borchert, H., Czock, K. H., et al. 1988, Nucl. Phys. A, 485, 621
Alexander, D. M., Brandt, W. N., Hornschemeier, A. E., et al. 2001, AJ, 122, 2156
Aller, H. D., Aller, M. F., Latimer, G. E., & Hodge, P. E. 1985, ApJS, 59, 513

Andrejscheff, W., Kohstall, C., von Brentano, P., et al. 2001, Phys. Lett. B, 506, 239
Arav, N., Shlosman, I., & Weymann, R. J. 1997, Mass Ejection from Active Galactic Nuclei, ed. N. Arav, I. Shlosman, & R. J. Weymann, ASP CS-128
Arav, N., Korista, K. T., de Kool, M., et al. 1999, ApJ, 516, 27
Arav, N., Korista, K. T., & de Kool, M. 2002, ApJ, 566, 699
Arav, N., Kaastra, J., Steenbrugge, K., et al. 2003, ApJ, 590, 174
Arav, N., Kaastra, J., Kriss, G. A., et al. 2005, ApJ, 620, 665
Aschenbach, B., Grosso, N., Porquet, D., & Predehl, P. 2004, A&A, 417, 71
Atoyan, A. M., & Aharonian, F. A. 1996, MNRAS, 278, 525
Axel, P. 1962, Phys. Rev., 126, 671
Axel, P., Min. K., Stein, N., & Sutton, D. C. 1963, Phys. Rev. Lett., 10, 299
Babilon, M., Hartmann, T., Mohr, P., et al. 2002, Phys. Rev. C, 65, 037303
Baganoff, F. K., Bautz, M. W., Brandt, W. N., et al. 2001, Nature, 413, 45
Baganoff, F. K., Maeda, Y., Morris, M., et al. 2003, ApJ, 591, 891
Ballo, L., Maraschi, L., Tavecchio, F., et al. 2002, ApJ, 567, 50
Band, D., Matteson, J., Ford, L., et al. 1993, ApJ, 413, 281
Barger, A. J., Cowie, L. L., Mushotzky, R. F., & Richards, E. A. 2001, AJ, 121, 662
Baring, M. 1994, IAUS, 159, 343
Barlow, T. A. 1997, in Proc. Mass Ejection From AGN, ed. N. Arav, I. Shlosman, & R. J. Weymann, ASP CP128, 13
Bassani, L., Dadina, M., Maiolino, R., et al. 1999, ApJS, 121, 473
Bauwens, F., Bryssinck, J., De Frenne, D., et al. 2000, Phys. Rev. C, 62, 024302
Begelman, M. 1999, in the Proc. of the Colloquium, The Most Distant Radio Galaxies, Amsterdam, 15–17 Oct., 1997, Royal Netherlands Academy of Arts and Sciences, ed. H. J. A. Röttgering, P. N. Best, & M. D. Lehnert, 173
Berg, U. E. P., Weinhard, K., & Wolf, H. 1975, Phys. Rev. C, 11, 1851
Bertoldi, F., Cox, P., Neri, R., et al. 2003, A&A, 406, L47
Bertsch, D. L., Dame, T. M., Fichtel, C. E., et al. 1993, ApJ, 416, 587
Bethe, H. A. 1937, Rev. Mod. Phys., 9, 71
Bianchi, N., Muccifora, V., de Sanctis, E., et al. 1996, Phys. Rev. C, 54, 1688
Bicknell, G. V., Dopita, M. A., & O'Dea, C. P. O. 1997, ApJ, 485, 112
Bicknell, G. V., Sutherland, R. S., van Breugel, W. J. M., et al. 2000, ApJ, 540, 678
Blandford, R. D., & Königl, A. 1979, ApJ, 232, 34
Blandford, R. D. 2000, Roy. Soc. London, Phil. Trans. A, 358, 811
Bloemen, H., Hermsen, W., Swanenburg, B. N., et al. 1994, ApJS, 92, 419
Bloemen, H., Morris, D., Knödlseder, J., et al. 1999, ApJ, 521, L137
Bloemen, H., Bennett, K., Collmar, W., et al. 2000, AIP CP-510, 586
Bloom, S. D., Bertsch, D. L., Hartman, R. C., et al. 1997, ApJ, 490, L145
Böttcher, M., & Bloom, S. D. 2000, AJ, 119, 469
Bohr, A., & Mottelson, B. R. 1975, Nuclear Structure II (New-York: Benjamin)
Brandt, W. N., Hornschemeier, A. E., Alexander, D. M., et al. 2001, AJ, 122, 1
Burns, M. L., & Lovelace, R. V. E. 1982, ApJ, 262, 87
Caraveo, P., Bignami, G. F., Mignani, R., & Taff, L. G. 1996, A&AS, 120C, 65
Carilli, C. L., Lewis, G. F., Djorgovski, S. G., et al. 2001, Science, 300, 773
Catanese, M., Akerlof, C. W., Biller, S. D., et al. 1997, ApJ, 480, 562
Celotti, A., Kuncic, Z., Rees, M. J., & Wardle, J. F. C. 1998, MNRAS, 293, 288
Cha, A. N., & Sembach, K. R. 2000, ApJS, 126, 399
Chambers, J., Zaremba, E., Adams, J. P., & Castel, B. 1994, Phys. Rev. C, 50, R2671
Chapuran, T., Starr, R., Vodhane, R., & Brussel, M. K. 1984, Phys. Rev. C, 30, 54
Chupp, E. L. 1976, Gamma-Ray Astronomy Geophysics and astrophysics monographs, 14 (Dordrecht: Reidel Publ. Co.)
Churchill, C. W., Schneider, D. P., Schmidt, D. P., & Gunn, J. E. 1999, AJ, 117, 2573
Collmar, W., Bennett, K., Bloemen, H., et al. 1997, A&A, 328, 33
Collmar, W. 2003, in Proc. High Energy Blazar Astronomy, ed. L. O. Takalo, & E. Valtaoja, ASP CP299, 29
Comastri, A., Setti G., Zamorani, G., & Hasinger, G. 1995, A&A, 296, 1
Comastri, A. 2004 [arXiv:astro-ph/0403693]
Conner, A. L., Atwater, H. F., Plassmann, H., & McCrary, J. H. 1970, Phys. Rev. A, 1, 539
Coppi, P. S., & Aharonian, F. A. 1999, APh, 11, 35
Corbett, E. A., Robinson, A., Axon, D. J., et al. 1996, MNRAS, 281, 737
Cotton, W. D., Counselman, C. C., III, Geller, R. B., et al. 1979, ApJ, 229, L115
Courvoisier, T. J.-L. 1998, A&AR, 9, 1
Crawford, C. S., Gandhi, P., Fabian, A. C., et al. 2002, MNRAS, 333, 809
Dawson, S., McCrady, N., Stern, D., et al. 2003, AJ, 125, 1236
de Kool, M., Arav, N., Becker, R. H., et al. 2001, ApJ, 548, 609
Dermer, C. D. 1995, ApJ, 446, L63
Dermer, C. D., & Schlikeiser, R. 1993, ApJ, 416, 458
Dermer, C. D., & Schlikeiser, R. 1994, ApJS, 90, 945
de Jager, O. C., Harding, A. K., Michelson, P. F., et al. 1996, ApJ, 457, 253
de Vries, C. P., den Herder, J. W., Kaastra, J. S., et al. 2003, A&A, 404, 959
Elitzur, M., Nenkova, M., & Ivecic, Z. 2003 [arXiv:astro-ph/0309040]
Enders, J., von Brentano, P., Eberth, J., et al. 1998, Nucl. Phys. A, 636, 139
Eramzhyan, R. A., Ishkhanov, B. S., Kapitonov, I. M., & Neudatchin, V. G. 1986, Phys. Rep., 136, 229
Esposito, J. A., Bertch, D. L., Chen, A. W., et al. 1999, ApJS, 123, 203
Fabian, A. C. 1999, MNRAS, 308, L39
Fabian, A. C., Sanders, J. S., Crawford, C. C., & Ettori, S. 2003, MNRAS, in press
Fabian, A. C. 2004 [arXiv:astro-ph/0410589]
Fang, T., Marshall, H., Lee, J. C., et al. 2002, ApJ, 572, L127
Fang, T., Sembach, K. R., & Canizares, C. R. 2003, ApJ, 586, L49
Fatuzzo, M., & Melia, F. 2003, ApJ, 596, 1035
Fichtel, C. E., & Trombka, J. I. 1981, Gamma Ray Astrophysics NASA SP-453
Fiedler, R., Dennison, B., Johnston, K. J., et al. 1994, ApJ, 430, 581
Fierro, J. M., Michelson, P. F., Nolan, P. L., & Thompson, D. J. 1998, ApJ, 494, 734
Freeman, P. E., Graziani, C., Lamb, D. Q., et al. 1999, ApJ, 524, 753
Freudenreich, H. T. 1998, ApJ, 492, 495
Ganguly, R., Eracleous, M. C., Charlston, J. C., & Churchill, C. W. 1999, AJ, 117, 2594
Genzel, R., Schödel, R., Ott, T., et al. 2003, Nature, 425, 934
George, I. M., Turner, T. J., Netzer, H., et al. 1998, ApJS, 114, 73
Georganopoulos, M., & Kazanas, D. 2004, ApJ, 604, L81
Ghez, A. M., Wright, S. A., Matthews, K., et al. 2004, ApJ, 601, L159
Giacconi, R., Rosati, P., Tozzi, P., et al. 2001, ApJ, 551, 624
Gilli, R., Risaliti, G., & Salvati, M. 1999, A&A, 347, 424

Gilli, R., Salvati, M., & Hasinger, G. 2001, A&A, 366, 407
Goldwurm, A., Brion, E., Goldoni, P., et al. 2003, ApJ, 584, 751
Grove, J. E., & Johnson, W. N. 1997, IAU Circ., 6705
Gruber, D. E., Heindl, W. A., Rothschild, R. E., et al. 2001, ApJ, 562, 499
Guianazzi, M., Siemigienowska, A., Rodriguez-Pascual, P., & Stanghellini, C. 2004 [arXiv:astro-ph/0402639]
Hagiwara, K., Hikasa, K., Nakamura, K., et al. 2002, Phys. Rev. D, 66, 010001-1
Halpern, J., Eracleous, M., Mukherjee, R., et al. 2001, ApJ, 551, 1016
Hanna, S. S., & Meyer-Schützmeister, L. 1959, Phys. Rev., 115, 986
Hartman, R. C., Bertch, D. L., Bloom, S. D., et al. 1999, ApJS, 123, 79
Hartmann, T., Enders, J., Mohr, P., et al. 2000, Phys. Rev. Lett., 85, 274
Hartmann, T., Enders, J., Mohr, P., et al. 2002, Phys. Rev. C, 65, 034301
Hasinger, G., Altieri, B., Arnaud, M., et al. 2001, A&A, 365, L45
Hayward, E. 1977, Lecture Notes in Physics, ed. S. Costa, & C. Schaerf, 61, 340 (Berlin-Heidelberg: Springer-Verlag)
Hubbell, J. H. 1971, Atomic Data, 3, 241
Hubbell, J. H., Gerstenberg, H. M., & Saloman, E. B. 1986, Bibliography of Photon Total Cross Section (Attenuation Coefficient) Measurements 10 eV to 13.5 GeV, NBSIR No. 86-3461
Hughes, E. B., Hofstadter, R., Rolfe, J., et al. 1980, IEE Trans. Nucl. Sci., NS-27, 364
Iwasawa, K., Fabian, A. C., & Ettori, S. 2001, MNRAS, 321, L15
Iyudin, A. F., Böhringer, H., Dogiel, V., & Morfill, G. 2004, A&A, 413, 817
Iyudin, A. F., Burwitz, V., Greiner, J., DiCocco, G., & Larsson, S. 2005, in Proc. Int. Conference, Baryons in Dark Matter Halo, 5–9 October 2004, Novigrad, Croatia, PoS, SISSA, ed. R. J. Dettmar, U. Klein, & P. Salucci; and [arXiv:astro-ph/0501039]
Jorstad, S. G., & Marscher, A. P. 2003, in Proc. High Energy Blazar Astronomy, ed. L. O. Takalo, & E. Valtaoja, ASP CP299, 111
Kaiser, H., von Brentano, P., Caurier, E., et al. 2000, Nucl. Phys. A, 669, 368
Kanbach, G., Bertsch, D. L., Fichtel, C. E., et al. 1988, Space Sci. Rev., 49, 69
Kaspi, S., Brandt, W. N., George, I. M., et al. 2002, ApJ, 574, 643
Kauffmann, G., Heckman, T. M., Tremonti, C., et al. 2003, MNRAS, 346, 1055
King, A. R., & Pounds, K. A. 2003, MNRAS, 345, 657
Komissarov, S. S., & Lyubarsky, Y. E. 2003, MNRAS, 344, L93
Koyama, K., Maeda, Y., Sonobe, T., et al. 1996, PASJ, 48, 249
Kuiper, L., Hermsen, W., Bennett, K., et al. 1996, A&AS, 120, 73
Lichti, G. G., Balonek, T., Courvoisier, T. J.-L., et al. 1995, A&A, 298, 711
Lutz, D., Sturm, F., Genzel, R., et al. 2002, ASP CS, 258, 39
MacCormick, M., Audit, G., D'Hose, N., et al. 1996, Phys. Rev. C, 53, 41
MacCormick, M., Habermann, J., Ahrens, J., et al. 1997, Phys. Rev. C, 55, 1033
Madejski, G. M., Sikora, M., Jaffe, T., et al. 1999, ApJ, 521, 145
Madau, P., Ghisellini, G., & Fabian, A. C. 1994, MNRAS, 270, L17
Maeda, Y., Baganoff, F. K., Feigelson, E. D., et al. 2002, ApJ, 570, 671
Mainieri, V., Bergeron, J., Hasinger, G., et al. 2002, A&A, 393, 425
Maiolino, R., Salvati, M., & Bassani, L. 1998, et al. A&A, 338, 781
Maiolino, R., Juarez, Y., Mujica, R., et al. 2003, MNRAS, 344, L59
Mannheim, K. 1993, A&A, 269, 67
Marscher, A. P., Jorstad, S. G., Mattox, J. R., & Wehrle, A. E. 2002, ApJ, 577, 85
Matt, G., Fabian, A. C., Guainazzi, M., et al. 2000, MNRAS, 318, 173
Matt, G., Guianazzi, M., & Maiolino, R. 2003, MNRAS, 342, 422
Mattox, J. R., Bertsch, D. L., Chiang, J., et al. 1996, ApJ, 461, 396
Mayer-Hasselwander, H. A., Bertsch, D. L., Dingus, B. L., et al. 1998, A&A, 335, 161
McNaron-Brown, K., Johnson, W. N., Jung, G. V., et al. 1995, ApJ, 451, 575
Moreh, R., Shlomo, S., & Wolf, A. 1970, Phys. Rev. C, 2, 1144
Moreh, R., Sellyey, W. C., Sutton, D. C., et al. 1988, Phys. Rev. C, 37, 2418
Muccifora, V., Bianchi, N., Deppman, A., et al. 1999, Phys. Rev. C, 60, 064616
Mücke, A., Protheroe, R. J., Engel, R. R., et al. 2003, Astropart. Phys., 18, 593
Mukherjee, R., Dingus, B. L., Gear, W. K., et al. 1996, ApJ, 470, 831
Mukherjee, R., Böttcher, M., Hartman, R. C., et al. 1999, ApJ, 527, 132
Mukherjee, R., Gotthelf, E. V., Halpern, J. P., & Tavani, M. 2000, ApJ, 542, 740
Mushotzky, R. F. 1997, in Proc., Mass Ejection from Active Galactic Nuclei, ed. N. Arav, I. Shlosman, & R. J. Weymann, ASP CS-128, 141
Mushotzky, R. F., Cowie, L. L., Barger, A. J., & Arnaud, K. A. 2000, Nature, 404, 459
Nandra, K., George, I. M., Mushotzky, R. F., et al. 1997, ApJ, 476, 70
Netzer, H. 1993, ApJ, 411, 594
Nicastro, F., Zesas, A., Drake, J., et al. 2002, ApJ, 573, 157
Nolan, P. L., et al. 1992, IEE Trans. Nucl. Sci., NS-39, 993
Nolan, P. L., Arzoumanian, Z., Bertsch, D. L., et al. 1993, ApJ, 409, 697
Nolan, P. L., Tompkins, W. F., Grenier, I. A., & Michelson, P. F. 2003, ApJ, 597, 615
Norman, C., Hasinger, G., Giacconi, R., et al. 2002, ApJ, 571, 218
Omont, A., Cox, P., Bertoldi, F., et al. 2001, A&A, 374, 371
Oros, A. M., Heyde, K., De Coster, C., & Decroix, B. 1998, Phys. Rev. C, 57, 990
Page, M. J., Stevens, J. A., Ivison, R. J., & Carrera, F. J. 2004 [arXiv:astro-ph/0407171]
Pedlar, A., Anantharamaiah, K. R., Ekers, R. D., et al. 1989, ApJ, 342, 769
Pica, A. J., Smith, A. G., Webb, J. R., et al. 1988, AJ, 96, 1215
Pietralla, N., Weller, H. R., Litvinenko, V. N., Ahmed, M. W., & Tonchev, A. P. 2002, NIM A483, 556
Piner, B. G., Unwin, S. C., Wehrle, A. E., et al. 2003, ApJ, 588, 716
Porter, C. E., & Thomas, R. G. 1956, Phys. Rev., 104, 483
Porquet, D., Predehl, P., Aschenbach, B., et al. 2003, A&A, 407, L17
Pozzo, M., Jeffries, R. D., Naylor, T., et al. 2000, MNRAS, 313, L23
Pounds, K. A., Reeves, J. N., King, A. R., et al. 2003, MNRAS, 345, 705
Proga, D. 2003, ApJ, 585, 406
Purcell, W. R., Cheng, L.-X., Dixon, D. D., et al. 1997, ApJ, 491, 725
Ravasio, M., Tagliaferri, G., Ghisellini, G., et al. 2003, A&A, 408, 479
Reeves, J. N., O'Brien, P. T., & Ward, M. J. 2003, ApJ, 593, L65
Risaliti, G., Maiolino, R., & Salvati, M. 1999, ApJ, 522, 157
Risaliti, G., Elvis, M., & Nicastro, F. 2002, ApJ, 571, 234
Rosati, P., Tozzi, P., Giacconi, R., et al. 2002, ApJ, 566, 667
Rossi, B., & Greisen, K. 1941, Rev. Mod. Phys., 13, 240
Sambruna, R. M., Urry, C. M., Tavecchio, F., et al. 2001, ApJ, 549, 161
Savage, R. D., Sembach, K. R., Jenkins, E. B., et al. 2000, ApJ, 548, 27

Savage, R. D., Sembach, K. R., Wakker, B. P., et al. 2003, ApJS, 146, 125
Schönfelder, V., Aarts, H., Bennett, K., et al. 1993, ApJS, 86, 657
Schönfelder, V., Bennett, K., Blom, J. J., et al. 2000, A&AS, 143, 145
Setti, G., & Woltjer, L. 1989, A&A, 224, L21
Silk, J., & Rees, M. 1998, A&A, 331, L1
Snowden, S. L., Egger, R., Freyberg, M. J., et al. 1997, ApJ, 485, 125
Sofue, Y., Inoue, M., Handa, T., et al. 1986, PASJ, 38, 475
Solodukhov, G. V. 1976, Lect. Notes Phys., 62, v. II, 216
Stern, D., Tozzi, P., Stanford, S. A., et al. 2002, AJ, 123, 2223
Strauss, M. A., Huchra, J. P., Davis, M., et al. 1992, ApJS, 83, 295
Strong, A. W., Bennett, K., Bloemen, H., et al. 1993, A&AS, 97, 133
Suzuki, Y., Ikeda, K., & Sato, H. 1990, Prog. Theor. Phys., 83, 180
Telfer, R. C., Kriss, G. A., Zheng, W., et al. 1998, ApJ, 509, 132
Thompson, D. J., Bertsch, D. L., Fichtel, C. E., et al. 1993a, ApJS, 86, 629
Thompson, D. J., Bertsch, D. L., Dingus, B. L., et al. 1993b, ApJ, 415, L13
Thompson, D. J., Harding, A. K., Hermsen, W., & Ulmer, M. P. 1997, AIP CP410, 39
Tripp, T. M., Savage, R. D., & Jenkins, E. B. 2000, ApJ, 534, L1
Tsuchiya, K., Enomoto, R., Ksenofontov, L. T., et al. 2004, ApJ, 606, L115
Türler, M., Paltani, S., Courvoisier, T. J.-L., et al. 1999, A&AS, 134, 89
Urry, C. M., & Treister, E. 2004 [arXiv:astro-ph/0411099]
van der Meulen, R. D., Bloemen, H., Bennett, K., et al. 1998, A&A, 330, 321
van Dijk, R. 1996, Ph.D. Thesis, Amsterdam Univ.
Van Isacker, P., Nagarajan, M. A., & Warner, D. D. 1992, Phys. Rev. C, 45, R13
Varier, K. M., Nasiruddeen Kunju, M. A., & Madhusudanan, K. 1986, Phys. Rev. A, 33, 2378
Veilleux, S., Goodrich, R. W., & Hill, G. J. 1997, ApJ, 477, 631
Vignati, P., Molendi, S., Matt, G., et al. 1999, A&A, 349, L57
Voges, W., Aschenbach, B., Boller, Th., et al. 1999, A&A, 349, 389
von Montigny, C., Aller, H., Aller, M., et al. 1997, ApJ, 483, 161
Walter, F., Bertoldi, F., Carilli, C., et al. 2003, Nature, 424, 406
Webb, J. R., Carini, M. T., Clements, S., et al. 1990, AJ, 100, 1452
Wehrle, A. E., Piner, B. G., Unwin, S. C., et al. 2001, ApJS, 133, 297
Wilman, R. J., Fabian, A. C., Crawford, C. S., & Cutri, R. M. 2003, MNRAS, 338, L19
Zamorani, G., Maaccacaro, T., Giommi, P., & Tananbaum, H. 1984, ApJ, 278, 28
Zhao, J.-H., Young, K. H., Herrnstein, R. M., et al. 2003, ApJ, 586, L29
Zilges, A., Volz, S., Babilon, M., et al. 2002 [nucl-ex/0207016]

Online Material

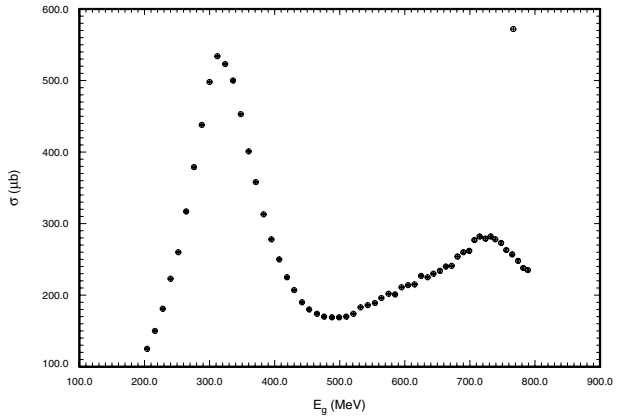

Fig. A.1. Gamma-ray absorption cross section on the proton in the region of Δ and N^* resonances (MacCormick et al. 1996). Here E_g is the photon energy.

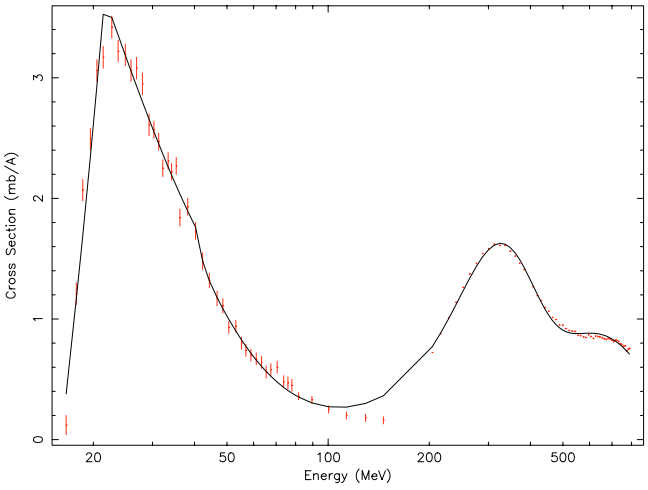

Fig. A.2. Gamma-ray absorption cross section on the ^{4}He in the region of the GDR, Δ and N^* resonances (MacCormick et al. 1997).

Appendix A: Cross sections of γ-ray interactions with nuclei

A.1. Total cross sections in the isobar region

At the photon energies exceeding the threshold for pion production, the total absorption cross section of the photon interacting with the individual nucleon or with a nucleus shows a remarkably universal feature, a resonance that corresponds to the isovector magnetic dipole transition that connects the nucleon and the Δ(1232) isobar. This resonance dominates the nuclear electromagnetic response at excitation energies of $E_\gamma >$ 200 MeV (Figs. A.1–A.3). The position of the Δ-resonance in the photon absorption cross section does not change for all nuclei from helium up to uranium. This position also coincides with the Δ-resonance maximum in the free γ-proton cross section. The only notable difference is the change of the Δ-resonance width from $FWHM \sim 160$ MeV for a proton to $FWHM \sim 300$ MeV for a nuclei. This $FWHM$ broadening happens because many more decay channels of the Δ isobar are open in the nuclei, like $\Delta N \rightarrow NN$, while in the free $\gamma p \rightarrow \Delta$ interaction, only $\Delta \rightarrow \pi N$ channel is open.

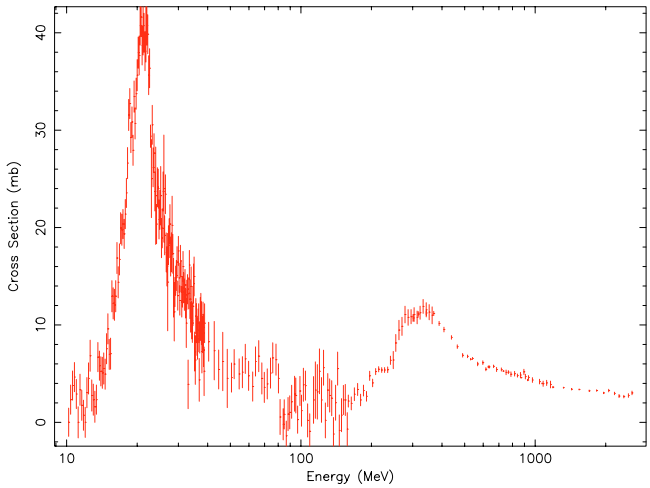

Fig. A.3. Gamma-ray absorption cross section on the ^{27}Al in the region of the giant dipole resonance (GDR) and Δ resonance (Ahrens et al. 1975; Bianchi et al. 1996; Muccifora et al. 1999).

The total absorption cross section of the photon in the Δ-isobar region was discussed in several papers. These cross sections have now been measured for a series of nuclei at photon energies ω up to approximately 200 GeV (Ahrens 1985; Fig. 39.17 in Hagiwara et al. 2002). The most complete survey of the data on $\sigma_{\gamma A}(\omega)$ with a list of references and a detailed discussion of the fitting procedure is given by Ahrens (1985). Some additional experimental results were discussed by Solodukhov (1976); see also MacCormick et al. (1996, 1997).

Typical results of the $\sigma_{\gamma A}(E_\gamma)$ measurements are shown in Figs. A.1–A.3. A comparison of the cross-section per nucleon for several nuclei demonstrates the universal behavior in the Δ-resonance region with characteristic nuclear damping, e.g. a decrease of the peak cross section value for all nuclei as compared with the same value for the isolated proton (Ahrens 1985). The peak value of the photon absorption cross section in the isobar resonance region happens to be at the same photon energy of $E_{\gamma 0} = 327 \pm 5$ MeV for all nuclei.

A.2. Total absorption cross section in the giant dipole resonance (GDR) region

The total absorption cross section ($\sigma_{\gamma T}$) of γ-quanta by nuclei was studied by nuclear physicists in order to gather important information for understanding the basic properties of nuclei (Ahrens et al. 1975; Ahrens 1985); for example, via the optical theorem $\sigma_{\gamma T}$ is linked to the imaginary part of the forward scattering amplitude, f_o, for the elastic scattering of photons:

$$\sigma_{\gamma T}\left(E_\gamma\right) E_\gamma \approx \mathrm{Im} f_o\left(E_\gamma\right). \quad (A.1)$$

The spin-averaged forward scattering amplitude can be determined by means of the dispersion relation if only $\sigma_{\gamma T}$ is known over a wide energy range. The moments of $\sigma_{\gamma T}$, S_a, – offer even more inclusive information than the cross section itself. The moments S_a are themselves defined by the following equation

$$S_a = \int_0^\infty \mathrm{d}W \sigma_{\gamma T}(W)\, W^a, \quad (A.2)$$

and are related to general properties of nuclei via the sum rules (Ahrens 1985). Among those moments, S_{-2} gives the static nuclear polarizability, S_{-1} measures the nuclear radius, and S_0 is the integrated absorption cross section which in theory counts the e^2/M that is involved in the interaction. We are interested only in the S_0, which is defined as

$$S_0\left(E_\gamma\right) = \int_0^{E_\gamma} \mathrm{d}W \sigma_{\gamma\mathrm{T}}\left(W\right). \tag{A.3}$$

S_0 is usually measured in units of the classical sum S_{cl}, which is the value that $S_0(\infty)$ would take if the nucleus were bound in a simple mean field potential. That is, if the nucleon-nucleon force were independent of nucleon momentum and free of exchange terms,

$$S_{\mathrm{cl}} = \frac{NZ}{A}\frac{2\pi^2 e^2}{M} = \frac{NZ}{A}\ \ 60\ \ \mathrm{MeV\ mb} \tag{A.4}$$

$$\frac{S_{\mathrm{cl}}}{A} \approx 15\ \ \mathrm{MeV\ mb}. \tag{A.5}$$

The ratio of the nuclear part to that of the atomic (electron) part of the gamma absorption cross sections changes from ~3–5% in the maximum of the GDR of ^{27}Al to 1.5–2.0% for ^{165}Ho and 2.0–2.5% for uranium (U). The shape of the GDR can typically be described by Lorenzian(s) with a width (Γ) that changes from ~4.5 MeV for ^{40}Ca, and 5.5 MeV for ^{16}O, to the values ~10 MeV for ^{27}Al and ~14 for ^{23}Na (Eramzyan et al. 1986; Ahrens et al. 1988).

Figures 1–3 show typical cases of photon absorption cross-section behaviour in the GDR region for ^{1}H, ^{4}He and ^{27}Al. Note the broadness of GDR for the photon absorption by ^{4}He (*FWHM* ~ 20 MeV). Also important is that GDR for ^{4}He extends up to 80 MeV at the 10% level of the cross-section value at the maximum of the GDR.

It is noteworthy to mention that all elements, except hydrogen, contribute to the absorption of gamma-rays in the GDR region. The lion's share of the GDR absorption happens to the abundant helium for solar composition. We also note that the energy dependences of GDR cross sections of deuteron (^{2}D), ^{3}H, and ^{3}He are shifted to lower energies relative to the cross section of other elements. For example, the GDR cross section for ^{2}D has its peak value at the energy of ~5 MeV, contrary to all other elements with $A \geq 4$ where the maximum of the GDR cross section is placed in the 20–30 MeV region (Eramzhyan et al. 1986). These different energy dependences of the gamma-ray absorption cross section of different elements may be used to evaluate an absorbing matter metallicity.

A.3. Total absorption cross section below the giant dipole resonance region

The behaviour of the photon absorption cross section below the GDR region is less well understood than that of the other two absorption processes, while the situation with resonance positions and strengths in this region, depending on the nuclei mass number, is more complicated than at higher energy resonances. In fact, the resonance-like absorption below

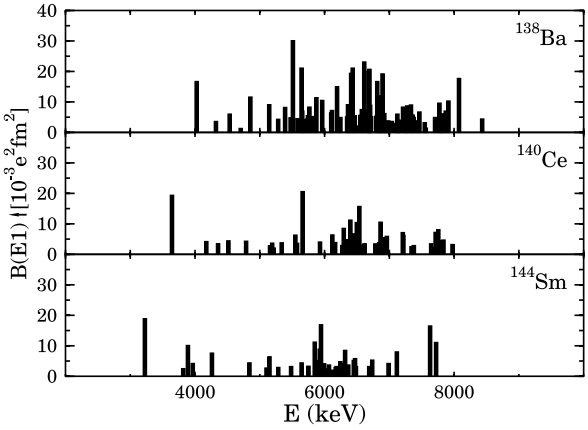

Fig. A.4. Electric dipole strength concentration in the region of the "pygmy" dipole resonance (PDR) (Zilges et al. 2002).

the photoproduction threshold can be produced: first, via photon absorption to the excitation level of the nuclei (Hanna & Meyer-Schützmeister 1959; Axel 1962; Hayward 1977) and, second, via the photon capture into the so-called "pygmy" dipole resonance (PDR) (Bohr & Mottelson 1975; Suzuki et al. 1990; Van Isacker et al. 1992; Enders et al. 1998; Bauwens et al. 2000; Kaiser et al. 2000; Andrejscheff et al. 2001; Babilon et al. 2002; Hartmann et al. 2002; Pietralla et al. 2002; Zilges et al. 2002).

The integrated cross section for the level excited by a γ-ray with energy $E = hc/\lambda$ is usually expressed in terms of the ground state width Γ_0:

$$\int \sigma_{\gamma\mathrm{T}}\left(E_\gamma\right)\mathrm{d}E_\gamma = \pi^2\lambda^2\left(\frac{2I_{\mathrm{e}}+1}{2I_{\mathrm{g}}+1}\right)\Gamma_0\left(I_{\mathrm{e}}{\rightarrow}I_{\mathrm{g}}\right). \tag{A.6}$$

For a ground state spin $I_{\mathrm{g}} = 0$ and for an excited state at $E^* = 7$ MeV with $I_{\mathrm{e}} = 1$ and $\Gamma_0 = 10$ eV, the integrated cross section is 2.35 MeV mb.

For a single element and a single level that decays only by direct γ-ray emission to the ground state, the cross section for the resonance fluorescence for γ-rays of energy E has the form

$$\sigma(E_\gamma) = \sigma_0 / \left\{1 + \left[\left(E_\gamma - E_r\right)/\frac{1}{2}\Gamma\right]^2\right\}, \tag{A.7}$$

where $\sigma_0 = \frac{1}{2\pi}\lambda^2(2I_{\mathrm{e}}+1)/(2I_{\mathrm{g}}+1)$ is the cross section exactly at resonance; I_{e} and I_{g} are the total angular momenta (spins) of the excited state and the ground state, respectively; E_{r} is the resonance energy, λ the corresponding wavelength, and Γ the natural width of the level. The factor 2 in the denominator of the expression for σ_0 is the multiplicity caused by two possible independent polarizations. An example of the σ_0 estimate for the resonant absorption by ^{14}N is given in Hanna & Meyer-Schützmeister (1959).

For a thin scatterer, the number of resonant-scattered quanta can be calculated by integrating the product of Eq. (7) and the incident spectrum over the energy. For the case of a thick scatterer, however, the thermal motion of absorbing nuclei has to be taken into account, and the general expression for effective cross section becomes rather complex (Bethe 1937). This expression may be simplified when the natural width Γ is

small compared with the Doppler width $\Delta = (E/c)(2kT/M)^{1/2}$, which results from the thermal motion of the absorbing (scattering) nuclei. This condition is fulfilled for the majority of important γ-ray transitions . The effective cross section has a pure "Doppler form":

$$\sigma_{\rm D} = K \exp\left\{-\left[\left(E_\gamma - E_r\right)/\Delta\right]^2\right\} = 44 \times \left(\frac{7\ {\rm MeV}}{E}\right)^2 \left(\frac{2I_{\rm e}+1}{2I_{\rm g}+1}\right) \frac{\Gamma_0}{\Delta}\ \ b, \quad (A.8)$$

where

$$K = \sigma_0 \left[\pi^{\frac{1}{2}} \Gamma/2\Delta\right]. \quad (A.9)$$

If the absorption cross section is integrated over an energy range that includes the entire resonance, one again obtains expression [6], independent of $\frac{\Delta}{\Gamma}$, which can be quantified as

$$\int \sigma_{\gamma {\rm T}}(E)\, {\rm d}E = 78 \times \left(\frac{7\ {\rm MeV}}{E_\gamma}\right)^2 \left(\frac{2I_{\rm e}+1}{2I_{\rm g}+1}\right) \Gamma_0\ \ b. \quad (A.10)$$

The value of Γ_0, e.g., of the excited state partial width corresponding to the de-excitation to the ground state, determines the contribution of each level to the average cross section.

We are interested mainly in analysing spectra with incident photons spread more or less uniformly over an energy interval ΔE_γ that includes n levels. The average level spacing D is equal to $\Delta E_\gamma/n$. Under such conditions the average cross section $\langle\sigma\rangle$ that will lead to the absorption may be written as

$$\langle\sigma\rangle = \frac{1}{\Delta E_\gamma} \sum_{i=1}^{n} ({\rm int})_i = \frac{\langle {\rm Int}_{I_{\rm e}} \rangle}{D_{I_{\rm e}}}. \quad (A.11)$$

In the case of a solar or other abundance mixture of elements that contribute to the nuclear resonance absorption via γ-nuclei interaction, one has to sum up contributions of different nuclei with usually differing energy levels and spins. Luckily enough, the majority of the abundant isotopes in ISM have the ground state with a zero spin value and a positive parity; e.g., ^{4}He, ^{12}C, ^{16}O, ^{24}Mg, ^{28}Si, and ^{56}Fe, all have a ground state with spin and parity of 0^+. All odd-even or even-odd nuclei have spins different from zero, but they are not among the most abundant elements.

The fact that most abundant elements have the same value of ground state spin simplifies, to some extent, any description of the level distribution around a photon energy of ~7 MeV for analysis of the photon absorption below a particle production threshold. To evaluate such a cross section one may use the energy level distribution described by the Porter-Thomas distribution for each of the typical ground state spin values (Axel 1962; Moreh et al. 1970).

$$\rho(Z) = \Gamma\left(\frac{Z}{2}\right)^{\left(\frac{\nu-2}{2}\right)} \exp^{-\nu\frac{Z}{2}}, \quad (A.12)$$

where $\Gamma\left(\frac{Z}{2}\right)$ is the usual Γ function, and $z = \frac{\Gamma_i}{\bar{\Gamma}_i}$, with the $\bar{\Gamma}_i$ as the average partial radiation width. For the number of exit channels of $\nu = 30$, the spread of level width is $0.7\Gamma_\gamma \leq \bar{\Gamma}_i \leq 1.4\Gamma_\gamma$. Here we have used $D_{I_{\rm e}}$ as the mean energy interval between n energy levels for nuclei with an excited state spin of $I_{\rm e}$.

For the cases with a mixture of absorbing elements having ground states of different spin and parity values, the nuclear resonance absorption cross section can be described by an equation

$$\langle\sigma\rangle = \sum_{I_{\rm e}} \frac{\langle {\rm Int}_{I_{\rm e}} \rangle}{D_{I_{\rm e}}} \sim \sum_{I_{\rm e}} \left(\frac{2I_{\rm e}+1}{2I_{\rm g}+1}\right) \frac{\langle \Gamma_0^q \rangle_{I_{\rm e}}}{\Gamma D_{I_{\rm e}}}, \quad (A.13)$$

which is valid when more than one value of $I_{\rm e}$ plays a role in the process of absorbing gamma-photons. Here $\langle\Gamma_0^q\rangle$ is an average value of the qth power of Γ_0 derived from the Porter-Thomas distribution (Porter & Thomas 1956). It gives the probability of finding a width Γ_0 among different levels that contribute to a resonance in an energy interval larger than the Doppler width of the resonance. This is mostly the case for γ-ray telescopes with moderate energy resolution, like COMPTEL.

The absorption cross section in the PDR region usually shows a peak in the photon strength function associated mainly with the isovector E1 absorption to the excited states. Figure 4 illustrates the strength distribution of the "pygmy" dipole resonances (E1) for heavy nuclei, like ^{138}Ba, ^{140}Ce, and ^{144}Sm (Zilges et al. 2002). Lighter nuclei like ^{51}V, ^{52}Cr, ^{40}Ca, ^{48}Ca, and ^{56}Fe also show this type of concentration of electric dipole strength in the region of 6–7 MeV of photon energy (Enders et al. 1998; Bauwens et al. 2000; Kaiser et al. 2000; Andrejscheff et al. 2001; Babilon et al. 2002; Hartmann et al. 2002; Pietralla et al. 2002).

New evidence of the PDR was delivered and discussed recently by Andrejscheff et al. (2001), which is based on an E1 strength concentration around ~6.5 MeV for even-even and closed shell nuclei. It is stated that this effect can be best understood in the boundaries of a nuclei "Dipole Core Polarization" suggested by Bohr & Mottelson (1975). The early conclusion that the levels in the peak of the cross section connect unusually strongly to the ground states in a number of nuclei remains valid until the present (see Axel et al. 1963; Berg et al. 1975; Moreh et al. 1988; Chambers et al. 1994; Oros et al. 1998; Bauwens et al. 2000; Andrejscheff et al. 2001; Babilon et al. 2002; Hartmann et al. 2002). However, systematic study of nuclides in this energy range up to the particle threshold has not yet been performed (Hartmann et al. 2002; Zilges et al. 2002).